(1)

CRACK GROWTH OF A TITANIUM-ALUMINIDE ALLOY UNDER THERMAL-MECHANICAL FATIGUE

THESIS

David G. Burgess
Captain, USAF

AFIT/GAE/AA/88D-3

DEPARTMENT OF THE AIR FORCE
AIR UNIVERSITY
AIR FORCE INSTITUTE OF TECHNOLOGY

Wright-Patterson Air Force Base, Ohio

AFIT/GAE/AA/88D-3

CRACK GROWTH OF A TITANIUM-ALUMINIDE ALLOY UNDER THERMAL-MECHANICAL FATIGUE

THESIS

David G. Burgess
Captain, USAF

AFIT/GAE/AA/88D-3

AFIT/GAE/AA/88D-3

CRACK GROWTH OF A TITANIUM-ALUMINIDE ALLOY UNDER THERMAL-MECHANICAL FATIGUE

THESIS

Presented to the Faculty of the School of Engineering

of the Air Force Institute of Technology

Air University

In Partial Fulfillment of the

Requirements for the Degree of

Master of Science in Aeronautical Engineering

David G. Burgess

Captain, USAF

December 1988

Preface

The major purpose of this thesis was to perform baseline Thermal-Mechanical-Fatigue (TMF) tests of a titanium-aluminide alloy, Ti_3Al. I could not have accomplished this without the help of Lt. John Pernot. John developed the hardware used in this investigation and provided valuable assistance in its operation. I would also like to thank Mr. Jay Anderson for his help in trouble-shooting the equipment.

Many thanks go to Dr. Theodore Nicholas, of the Air Force Materials Laboratory Metals Behavior Branch and Mr. Ted Fecke, AFWAL/POTA for sponsoring this work. I would like to especially thank Dr. Shankar Mall, for all his help in selecting test conditions, analyzing results, and editing this work.

Most of all I would like to thank my wife, [redacted] and daughters, [redacted] for their patience and understanding during the last 18 months.

Table of Contents

List of Figures

List of Tables

Abstract

New materials must be developed in order to increase the operating temperature of Air Force gas turbines. One of the materials under consideration is a titanium-aluminide alloy, Ti_3Al. Before this material can be used, its behavior under combined thermal-mechanical fatigue (TMF) conditions must be understood.

To understand this behavior, three 315-649^{o} C TMF tests and one 649^{o} C isothermal fatigue test with load hold time were conducted. Crack growth data from these tests were compared with each other as well as with crack growth data from four previous TMF and isothermal fatigue tests of the same material.

Two competing time-dependent crack growth mechanisms were present. Environmental degradation of the crack tip occurred when the material was exposed to points of maximum temperature and minimum load in the cycle. This accelerated the crack growth rates. Blunting of the crack tip due to creep occurred during hold times of maximum temperature and maximum load. This retarded crack growth rates.

Further TMF and isothermal fatigue tests are required to fully understand under what conditions these two time-dependent phenomena are present. This understanding is required before any TMF crack growth prediction model can be developed for this material.

CRACK GROWTH OF A TITANIUM-ALUMINIDE ALLOY UNDER THERMAL-MECHANICAL FATIGUE

I. Introduction

In order to increase the operating temperature of Air Force gas turbines, new materials must be developed which can withstand these higher temperatures. Since inherent flaws are contained in virtually all engine components, the ability to predict crack growth rates in these materials at these elevated temperatures is of primary importance. Engine components are subjected to simultaneous temperature and load variations; therefore there is an obvious need to investigate crack growth under thermal-mechanical fatigue (TMF).

Engineers must be able to predict accurately the crack growth under the engine thermal-mechanical cycling spectrum to determine if cracks of detectable size, and smaller, will grow to critical size during the engine lifetime. A typical spectrum includes variations in temperature, load magnitude, load frequency, and hold times as shown in Figure 1. At high temperatures, environmental degradation and/or creep can become important factors affecting crack growth. The very harsh environment that aircraft engine components face during service is difficult to recreate during a laboratory

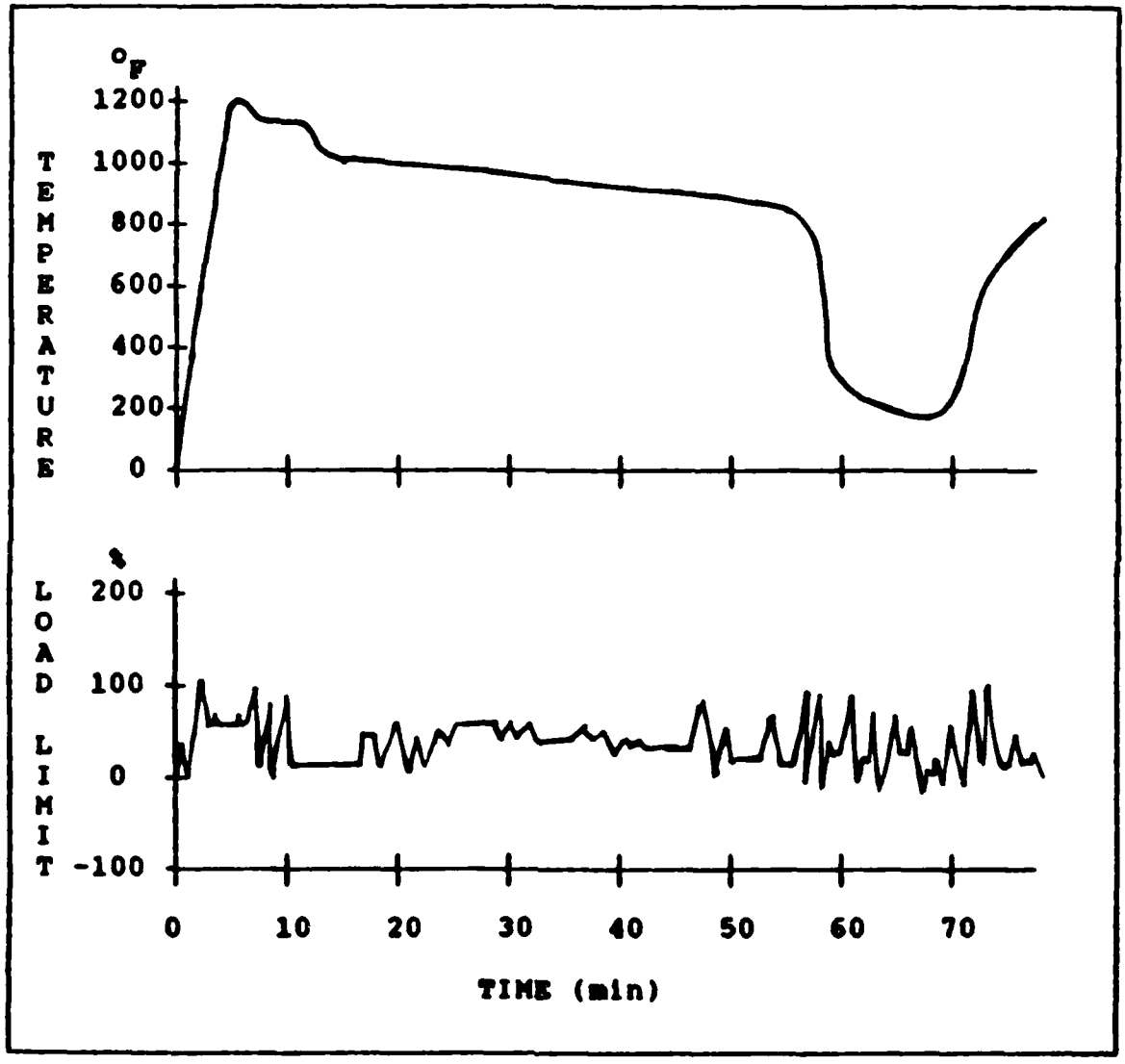

Fig. 1. Temperature and Loading Profiles of a Turbine Disk During a Typical Flight (5:2)

test. The TMF tests of prospective engine materials are one of the valuable tools available today to gage how well these materials will perform in an engine.

In a TMF test, the load and temperature are cycled simultaneously. These TMF tests, although quite useful in predicting crack growth rates under various conditions, are tedious and expensive to conduct. Therefore, the vast majority of fatigue growth testing of engine materials has been performed under isothermal conditions (1:346). A crack growth prediction model has been developed for Inconel 718 which is used in some engine components (2). This model is based on isothermal data and can predict crack growth under TMF conditions. In this approach, fatigue and sustained load data were collected under isothermal conditions and then this data were used to develop the model to predict crack growth under general TMF conditions. A limited number of TMF tests were then performed and the TMF data were used to validate the model (2:111). Based on the ability of the model to predict crack growth in these TMF tests, it was determined that the model could be used to predict crack growth in IN-718 under many varied and complex load and temperature combinations. Actual testing of components under all the various conditions would be both economically and physically prohibitive.

A titanium-aluminide alloy (Ti_3Al), alloy has recently been developed for use as a matrix in composites which can operate at the high temperatures required for high performance jet engines. This is a low density alloy with high specific strength and high temperature capabilities. The nickel-base superalloys have similar properties, but the Ti_3Al alloy has a lower operating temperature of approximately 649 C. The Ti_3Al alloy also promises component weight reduction with equal strength and is far less susceptible to combustion than conventional titanium alloys (3:1). Engine weight savings of up to 16 percent could be possible through extensive use of the Ti_3Al alloy (4:1). The United States also has substantial reserves of titanium, unlike the elements needed for the superalloys which are controlled by foreign sources.

Very limited fatigue data currently exists for this material and no attempt has been made to develop a crack growth prediction model. The overall goal of this present study was to develop a crack growth prediction model for the Ti_3Al alloy, which can be used under general TMF conditions. The more immediate goal was to gather baseline TMF and isothermal fatigue crack growth data, to be used in the development of this model. A test facility to conduct TMF tests has been recently developed by Pernot (5); he also gathered initial crack growth data in Ti_3Al under TMF conditions. Additional TMF and isothermal fatigue tests

were accomplished in this present investigation, to gain insight into the crack growth mechanisms present in this material.

II. Background

Mechanisms of Crack Growth

Fatigue Crack Growth. Pure fatigue crack growth is usually viewed as an elastic process, where a structure or test specimen is considered to act elastically on a macroscopic scale, while plastic deformation takes place on microscopic scale near the crack tip. During the loading portion of a fatigue cycle, the crack propagates and a small plastic region is formed near the crack tip. This plastic region occupies more volume than its elastic surroundings will allow and during the unloading portion of the cycle the region is compressed. Reversed plastic deformation occurs due to this compression and the crack tip is resharpened (6:61). The most common form of fatigue crack growth is a direct consequence of this cyclic blunting and resharpening of the crack tip. This type of behavior is seen in many engineering materials at room temperatures up to moderate temperatures (7:365).

Environmentally Enhanced Crack Growth. Crack growth rates can sometimes be greatly altered due to the environment in which the test takes place. When fatigue tests are conducted at elevated temperatures in air, crack growth rates usually increase with decreasing test frequency. At these high temperatures, the air can become an aggressive and

damaging environment to the material. Rapid oxidation of the newly formed crack tip, during the time the crack is opened, can cause embrittlement of the grain boundaries and provide an easier path for the crack to propagate (8:193). Coffin (9) observed that the room temperature and elevated temperature fatigue lives of a stainless steel, aluminum alloy, and nickel alloy were similar when the tests were performed in a vacuum. The vacuum test specimen showed transgranular failure, while specimen of the same materials tested in air at high temperature showed intergranular failure (9:1787). This environmentally assisted crack growth is sometimes called corrosion fatigue and is thermally activated. This is generally referred to as time-dependent crack growth. (10:235).

Creep crack growth. Creep can occur in engineering materials during exposure to sustained loads at high temperature. The effect of creep, in materials containing a crack, is to reduce the yield strength and increase the plastic zone size around the crack tip. In many cases, cavities form at grain boundaries due to plastic flow of the material due to creep. This cavitation will provide an easier path for the crack tip to travel and increase crack growth rates. Superalloys, stainless steels, copper, and other materials are known to exhibit this type of cavitation due to creep (11:215). Other materials, which are more ductile at the given temperature, may experience excessive

crack tip blunting due to the increased plasticity and have slower crack growth rates (12:173).

All three of these damage mechanisms can be present in a given material if the conditions of temperature, load, and environment are conducive. Their relative contributions are hard to quantify and make crack growth predictions of some materials very difficult. Their interaction will be explored in the next section.

Effects of Fatigue-Environment-Creep

Many engineering materials used today exhibit a complex fatigue-environment-creep damage mechanism when exposed to high temperature fatigue. Coffin (9) showed that the fatigue life of smooth fatigue specimen in air was reduced with a reduction in test frequency. The same type of specimen did not show a reduction in fatigue life with reduced test frequency, when the tests were performed in a vacuum. These results showed that these complex damage mechanisms are both time and environment dependent.

Crack Growth. Much experimental high temperature fatigue work has been done with several nickel-base superalloys. The most popular of these alloys has been Inconel-718 (IN-718). Many studies (2,13,14,15) have been conducted. These studies have included many different TMF cycles, isothermal fatigue, and sustained load tests. The influence of test temperature, environment, load ratio, test frequen-

cy, hold time, overload, and microstructure have been investigated in these studies. The time-dependent nature of the environmental damage was examined in these studies; the crack growth was accelerated during sustained load, low frequency, and hold time tests. These studies indicated that for high frequency cycles the environmental effect was negligible. This leads to the definition of cycle-dependent, time-dependent, and mixed-mode regions of crack growth as shown in Figure 2. These correspond to regions where the amount of crack propagation is dependent on the number of fatigue cycles, the elapsed time, and a combination of both, respectively. These studies also showed that, during time-dependent crack growth, the fracture changed from transgranular to intergranular. Floreen and Kane (16:1711-1749) performed a very thorough study of the effect of environment on the crack growth rate of IN-718. Not surprisingly, their results indicated that oxygen is the damaging element in air.

There can be a significant difference in time-dependent crack growth between different alloys. Cowles and others (17:305-315) performed 649^{o} C isothermal fatigue tests on seven different aircraft engine alloys. Their tests showed these alloys had similar crack growth rates at .33 hertz, but had growth rates which differed by a factor of 100 when a 900 second hold time was added to the fatigue cycle. These materials exhibited similar crack growth in the

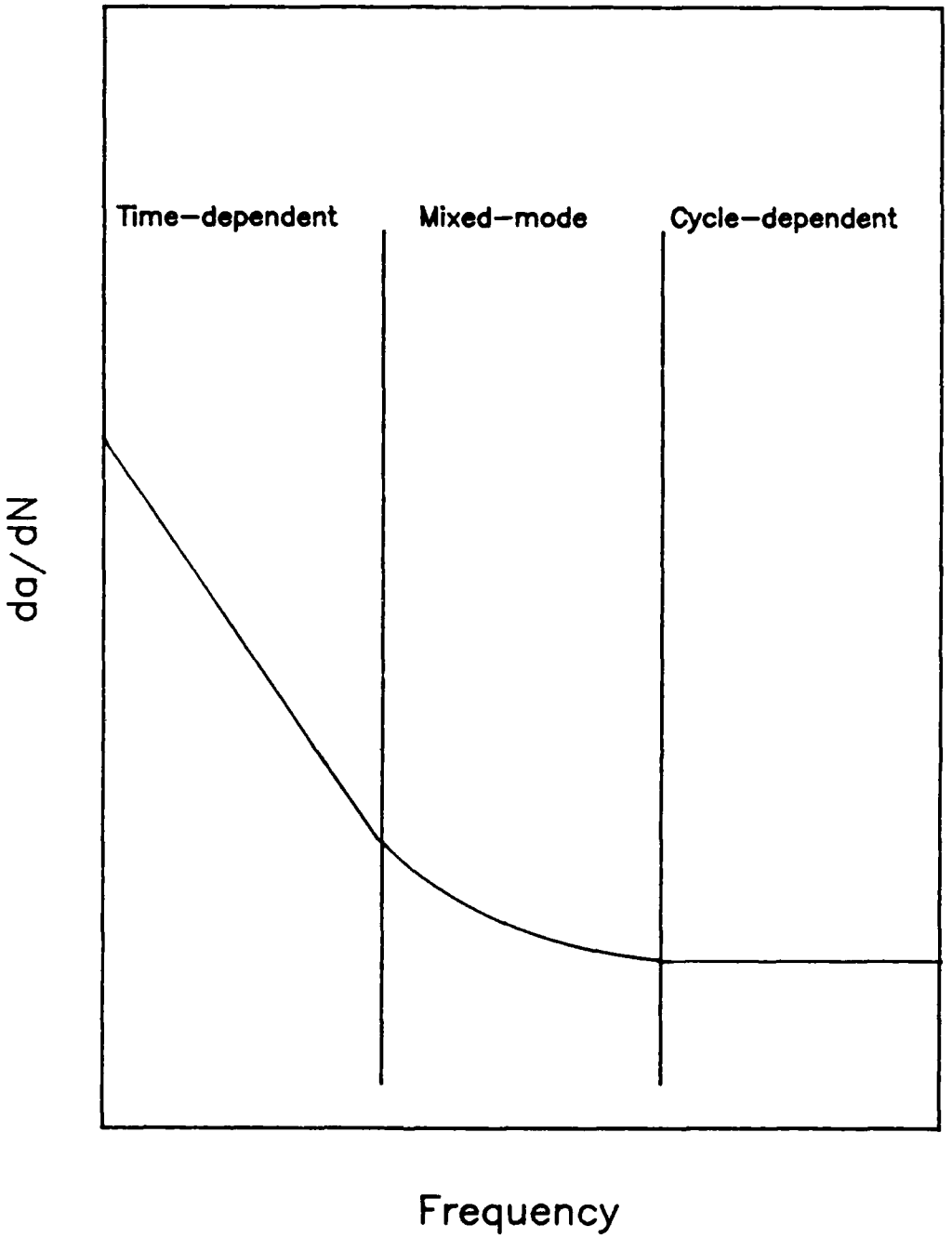

Fig. 2. Effect of Frequency on Crack Growth Rates

cycle-dependent region, but differed significantly in the time-dependent region.

The source of the accelerated time-dependent crack growth due to fatigue-environment-creep damage is not very well understood. This is true even in the case of the superalloys, for which there is a large amount of crack growth data available. Limited or no data exists in these areas for the Ti_3Al alloy used in this present study.

Another factor, which complicates the understanding and modeling of crack growth under such conditions, is the competition between the environmentally assisted crack growth and crack tip blunting caused by creep. Creep is the time-dependent deformation and subsequent reduction in yield strength which occurs, or can occur, in materials under sustained load. This is usually more prevalent at high temperatures. The effects of temperature on crack growth are to increase the crack growth rates, and to increase crack tip plasticity due to the reduced yield strength. The effects of load hold time at high temperature are to accelerate the crack growth in environmentally sensitive materials, and to increase crack tip blunting through creep (18:1375-1381). The effects of sustained load cracking due to environment and creep due to hold time at temperature can cancel each other, resulting in no net effect on crack growth rates. In other words, an isothermal fatigue test might show the same crack growth rates with or without hold

time due to this canceling effect. An environmentally sensitive material which also creeps at high temperature might demonstrate the behavior shown in Figure 3. During the fatigue portion of the test the crack propagates at a rate da/dt equal to m. During the hold time, the crack undergoes environmentally enhanced crack growth which may be eventually arrested due to the large plastic zone size due to creep. As the next fatigue portion begins, the growth rate is retarded to a value less than m by this creep blunting. In this case, the increased plasticity makes the crack behave as it would if it had experienced an overload. If the fatigue portion contains enough cycles, the effect of the blunted crack tip will eventually diminish to zero and the growth rate will again reach the original m value. The overall crack growth, da/dt, for the case depicted in Figure 3, shows the combination of sustained load cracking and crack tip blunting due to creep to be greater than if no hold time had been inserted (pure fatigue). It is not unlikely to suspect that the creep effects could be greater than the environmental effects, and the overall growth rate could be lower than that of pure fatigue.

The variation of temperature within a TMF test can also cause many varied and complicated mechanisms for crack growth. The interaction of load and temperature during a TMF cycle makes the prediction of crack growth under such conditions even more difficult. For TMF tests the phase

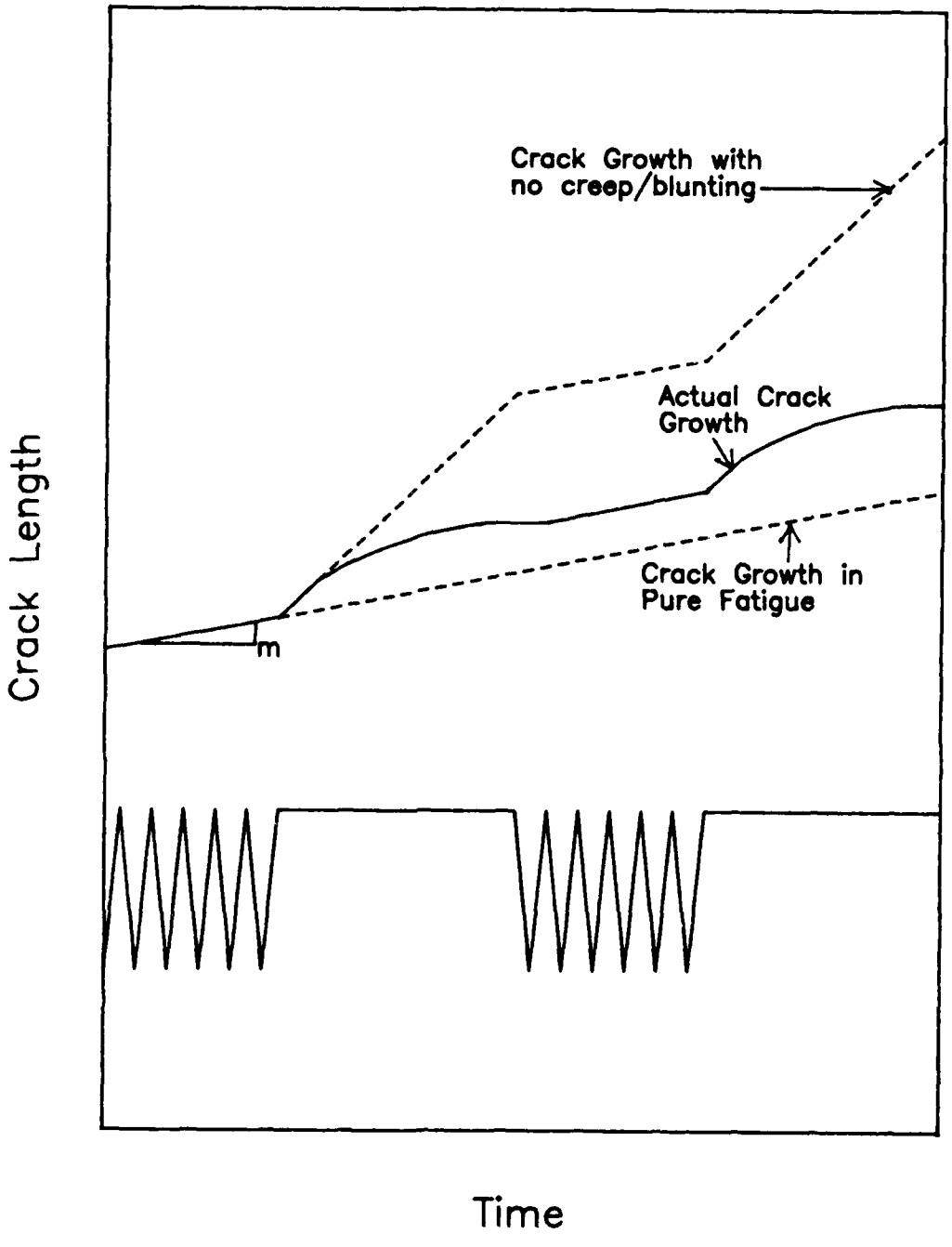

Fig. 3. Possible Damage Mechanisms During Fatigue Tests With Hold Time

angle plays an important part in the crack propagation. Not only does the value of the temperature and load at a given point effect the growth rate, but how the temperature and load are changing is also a factor. Heil (2:92-93) found that a 270° phase test and a 90° phase test produced much different crack growth rates in IN-718, even though they cover the same load/temperature paths as shown in Figure 4. He believed that the 270° phase test produced higher crack growth rates because the temperature was higher in that test, during the loading portion of the cycle. This provided credence to his theory that damage only occurred during the loading portion of the cycle.

Crack Growth Relations

Many mathematical relationships have been proposed to describe the relationship between crack growth rate (da/dN) and stress intensity range (ΔK). The three most widely used relationships are the Paris, Sinh, and modified sigmoidal (MSE) equations. The crack growth of most engineering materials can be represented by a log-log plot of da/dN vs. ΔK. Figure 5 shows a typical fatigue crack growth curve. Region I is the near threshold region where ΔK approaches ΔK threshold and da/dN decreases rapidly with decreasing ΔK. Region II is the region where an essentially linear relationship exists between da/dN and ΔK. Region III is the region where the crack growth is rapid and ΔK approaches the

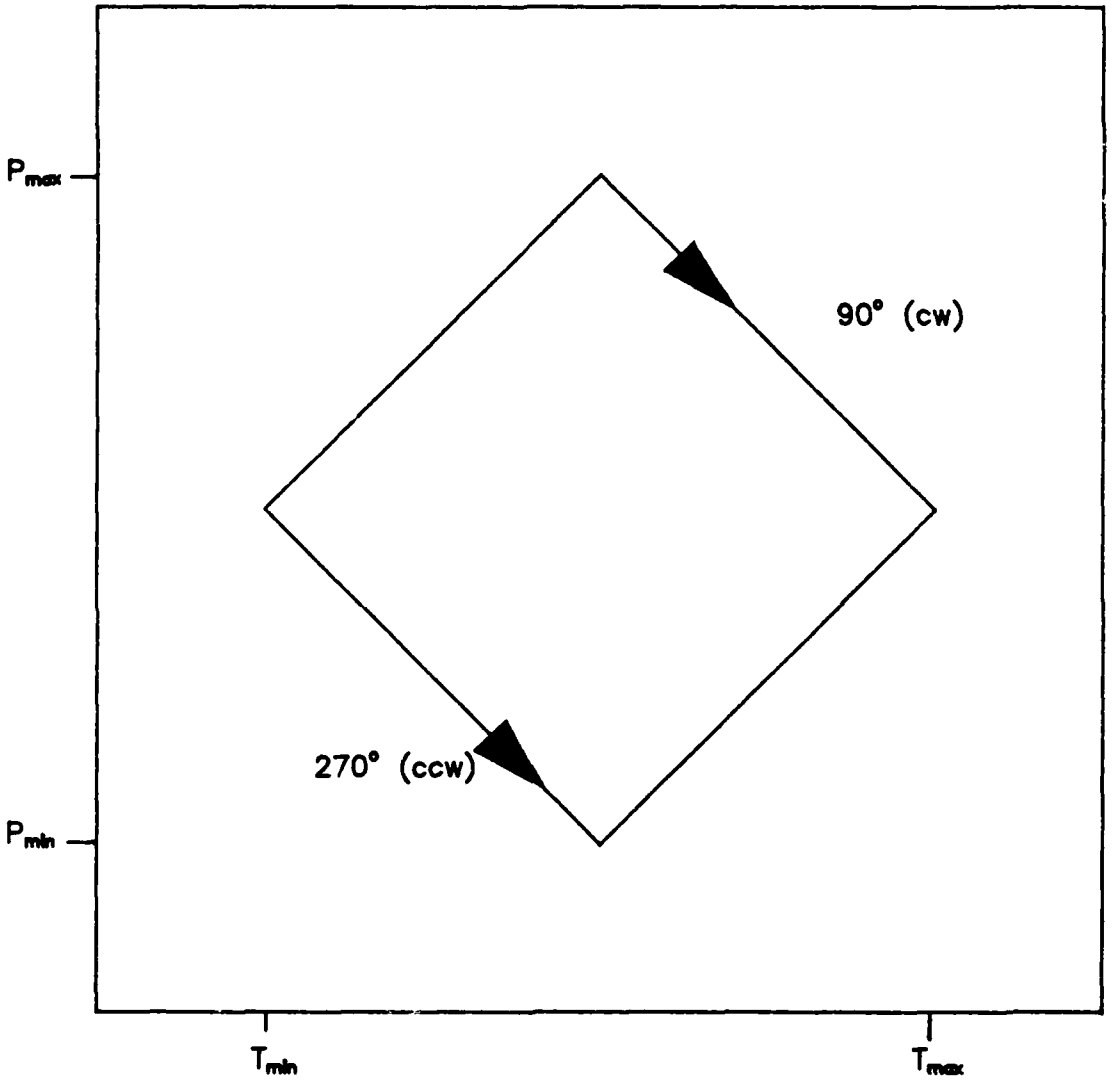

Fig. 4. Load and Temperature Paths for 270° and 90° Phase TMF tests

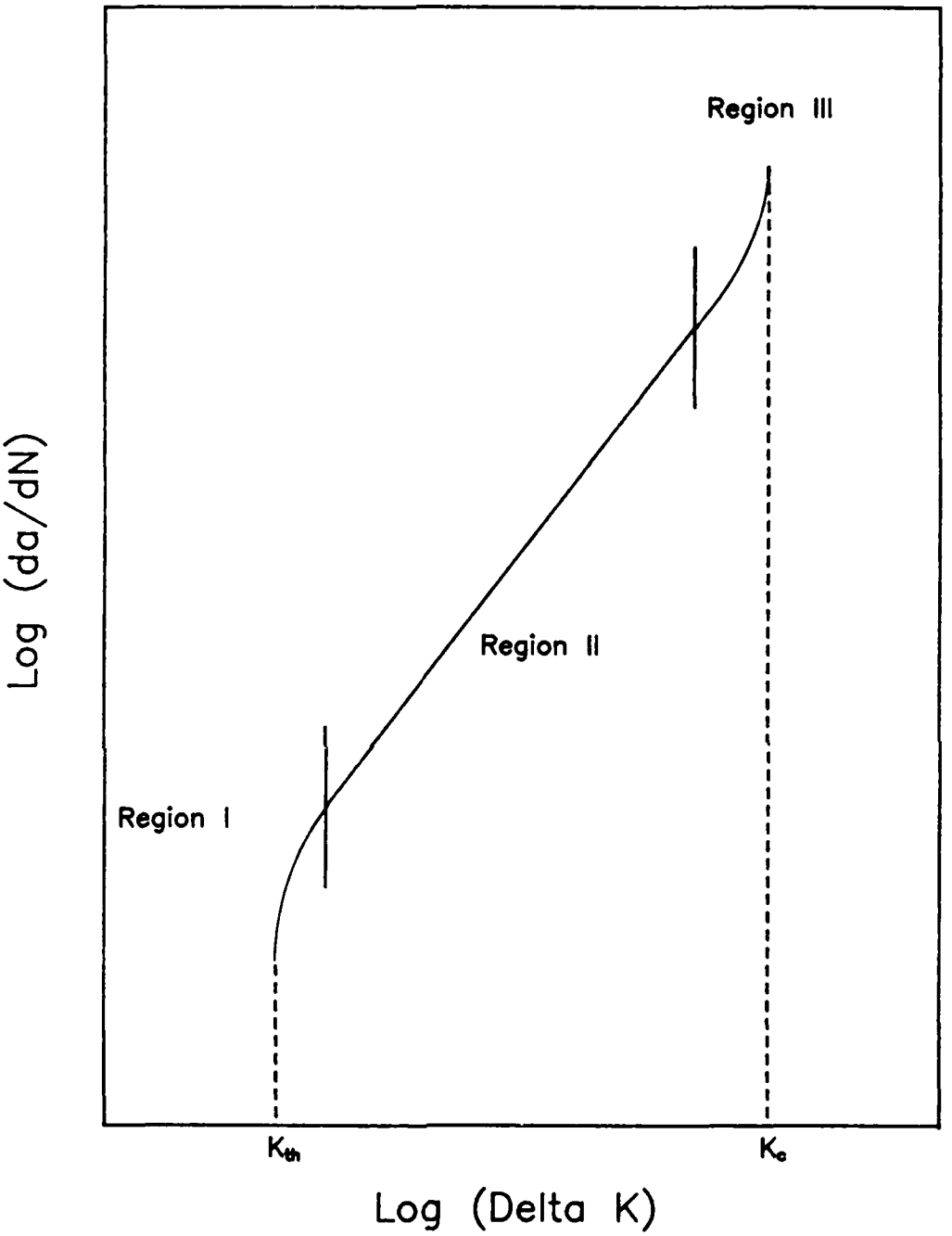

Fig. 5. Typical Crack Growth Curve

critical or failure value ΔK_c. All three of the mathematical relationships mentioned above consider the variation in the relationship of da/dN and ΔK in the three regions.

Paris Law. The first attempt to define a linear relationship between da/dN and ΔK was that of Paris (19). He proposed the following equation which is known as the Paris Law:

$$da/dN = C(\Delta K)^n \quad (1)$$

where C and n are material constants which can be determined from experimental data. The Paris Law defines Region II of the crack growth curve very well in most cases. It does not have the capability to define the transition between regions.

Sinh Curve. The hyperbolic sine (Sinh) curve for crack growth representation was first developed by Pratt and Whitney. It has been used to model the crack growth rates of several structural materials. The Sinh crack growth curve is:

$$\log(da/dN) = C_1 \sinh(C_2(\log\Delta K + C_3)) + C_4 \quad (2)$$

where C_1 is a material constant and C_2, C_3, and C_4 are functions of the test parameters: frequency, load ratio, and temperature.

Modified Sigmoidal Equation. The modified sigmoidal equation (MSE) has also been used to model the relationship between da/dN and ΔK. The MSE equation is:

$$da/dN = \exp(B)(\Delta K/\Delta K_i)^P[\ln(\Delta K/\Delta K_{th})]^Q[\ln(\Delta K_c/\Delta K)]^D \quad (3)$$

where ΔK_{th} is the threshold value of ΔK, ΔK_c is the critical value of ΔK, ΔK_i is the value of ΔK at the inflection point, and B, P, Q, and D determine the slope, position and shape of the curve. The location of the inflection point is dependent on B, P and ΔK_{th}. This three term dependence makes it very difficult to determine the value of the coefficients. Some simplifications can be made, for instance Heil (2) made the curve symmetric about the inflection point. This allowed ΔK to be expressed as a function of ΔK_{th} and ΔK_i and the number of independent parameters was reduced from six to five.

Predicting Crack Growth at Elevated Temperatures

Due to the complicated and expensive nature of TMF testing, much effort has been put into constructing crack growth predictive models based on isothermal fatigue and sustained load crack growth data. Many of these efforts have made use of either the Paris Law, Sinh curve, modified sigmoidal equation, or other relation based on linear elastic fracture mechanics (LEFM). LEFM is considered to be

valid as long as the plastic zone surrounding the crack tip is small as compared to the crack length (6:15). If the plastic zone is too large to be ignored, the elastic-plastic fracture mechanics (EPFM) relations such as the J-integral or crack tip opening displacement (CTOD) must be used. Much more work has been done in the area of LEFM, using stress intensity factor range ΔK as a correlating factor, than in EPFM. No matter which type of analysis is used, the major goal of any effort is to construct a model which predicts TMF crack growth, but is based entirely on isothermal data.

Two types of models have been used to predict the time-dependent crack growth in the superalloys. Interpolative models describe the constants in the preceding crack growth equations as a function of load ratio, test frequency, hold time, temperature, or other test variables. Superposition models predict the cycle-dependent and time-dependent contributions separately and add the two contributions to obtain the total crack growth prediction.

An interpolative Sinh model was developed by Sims (20) and an interpolative sigmoidal model was developed by Utah (21). Both of these models were developed by determining the influence of temperature, hold time, frequency, and load ratios on the constants in their respective equations. Both of these models were able to predict region II crack growth of the superalloys during isothermal fatigue tests with or without hold times.

As mentioned earlier, the total crack growth of materials can be described using a superposition model; where the total crack growth rate is the sum of the cycle-dependent crack growth rate and the time-dependent crack growth rate as follows:

$$da/dN = (da/dN)_c + \Delta a \qquad (4)$$

where da/dN is the total crack growth, $(da/dN)_c$ is the cyclic contribution and Δa is the time-dependent contribution. This model was first proposed by Wei and Landes where they modeled the corrosion fatigue in high strength steels (22:25-46). They proposed that the total rate of fatigue crack growth rate in an aggressive environment, da/dN, could be considered as the sum of the fatigue crack growth rate in an inert environment, $(da/dN)_c$, and the integration of sustained load crack growth data in the same aggressive environment over the same load profile, Δa. Their work predicted crack growth rates due to environmental assisted fatigue during isothermal conditions. This type of model was later applied to elevated temperature crack growth of superalloys (23).

Miller developed a linear cumulative damage model for predicting crack growth rates in IN-718 under sustained loads where the temperature was cycled (24:172-179). The temperature was cycled between 537 and 649^{o} C, with various

frequencies and hold times. He performed baseline isothermal sustained load tests at 537, 593, and 649° C. Based on this data, he assumed a linear relationship between log da/dt and log temperature. From this, he derived the following expression for the average growth rate during a linear change of temperature from T_1 to T_2 at a given value of stress intensity:

$$\dot{a}_{av} = [(\dot{a}_2)(T_2) - (\dot{a}_1)(T_1)]/[(T_2 - T_1)(n + 1)] \qquad (5)$$

where $\dot{a}_1$ and $\dot{a}_2$ are the isothermal crack growth rates at T_1 and T_2 respectively, and n is the slope of the log da/dt vs. log temperature curve.

From this equation, he could predict the crack growth rate for any combination of linear temperature cycles or hold times. He simply divided each cycle into i linear segments and then used the following expression to find the predicted growth rate for the entire cycle:

$$\dot{a}_{cycle} = \left[\sum_i (\dot{a}_{av})_i t_i\right] / \left[\sum_i t_i\right] \qquad (6)$$

where $\dot{a}_{cycle}$ is the predicted crack growth rate for the entire cycle, $(\dot{a}_{av})_i$ is the average growth rate for the ith segment and t_i is the time of the ith segment. The

stress intensity could be incremented to allow Eq (6) to predict crack growth rates over an entire test. This process amounted to treating the temperature cycle as a series of short hold times at constant temperature. He ignored any transient effects from going from one temperature to another, and also ignored any residual effect which one cycle might have on the subsequent cycle. This simple linear summation model worked well for this material at these temperatures, where the effect of environment was negligible. His model predicted crack growth rates within a factor of two of the experimental results.

The model considered for use in this current test effort was the linear cumulative damage model for IN-718 which was developed by Heil (2). Heil's model was developed entirely from isothermal crack growth data, and was used to predict crack growth rates under TMF conditions. No load history or interaction of crack growth mechanisms were considered. He followed a concept of Nicholas and others (14), where a simple linear summation of damage effects was used to obtain the total crack growth rate. The model sums cycle-dependent, mixed-mode, and time-dependent damage contributions, as shown in Figure 2, to obtain total crack growth for a cycle. The following expression was used to determine the total crack growth rate:

$$da/dN = (da/dN)_c + (da/dN)_t + (da/dN)_m \quad (7)$$

where da/dN is the total crack growth rate, $(da/dN)_c$ is the cycle-dependent contribution, $(da/dN)_t$ is the time-dependent contribution, and $(da/dN)_m$ is the mixed mode contribution.

He used isothermal 427° C fatigue data to obtain the cycle-dependent contribution. This cycle-dependent data was collected at a test frequency of 10 hertz, which was high enough to be in the pure cycle-dependent region for this material. The mixed-mode contribution was then obtained from isothermal 538° C and 649° C fatigue data. He then used isothermal sustained load data at 538° C, 593° C, and 649° C to obtain the time-dependent contribution.

The cycle-dependent contribution, obtained from a low temperature and high frequency fatigue test, was assumed to be independent of both temperature and frequency. Heil fitted the MSE equation to the experimental data and obtained the MSE constants for the cycle-dependent contribution. The time-dependent contribution was assumed to be dependent on both temperature and frequency. This term was found by integrating the sustained load crack growth rate, as a function of temperature, over the loading portion of the cycle. He later revised his time-dependent contribution, by performing this integration over only the loading portion of the cycle where the crack tip velocity, da/dt, was increasing. Heil then conducted TMF tests at phase angles of

0^{o}, 90^{o}, 180^{o}, 225^{o}, 270^{o}, and 315^{o}. The temperature limits for these TMF tests were 427-649^{o} C. The data from these TMF tests were then used to validate his model; all of his model predictions were within a factor of two of the experimental results.

III. Experimental Equipment and Procedure

In order to perform the required TMF tests for this present study, a test system capable of simultaneously varying both load and temperature was required. The system developed by Pernot (5:21-49) was used and is described briefly here for the sake of completeness and brevity. The major components are described below.

Test System

The thermal-mechanical test equipment consisted of the following major components:

1.) 10 Kip Material Testing System (MTS) servohydraulic machine
2.) Zenith Z-248 computer
3.) Wavetek model 75 arbitrary waveform generator
4.) MTS controller and data display
5.) Micricon 82300 temperature control system
6.) Four quartz lamp heaters
7.) Eight type-K thermocouples
8.) Hewlett-Packard 3456A digital voltmeter
9.) Hewlett-Packard 6033A DC power supply
10.) Compressed cooling air system
11.) Cooling water system

12.) Traveling microscope with digital read-out

13.) Compact tension specimen

The test system used for these TMF tests consisted of a mechanical loading device, temperature control unit, and crack growth measurement instruments. A main computer was used to control the load and temperature and acquire the load, temperature, and crack length data. Figure 6 shows a diagram of the entire system. The mechanical loading was produced by a closed loop MTS servohydraulic loading and control system is shown in Figure 7. The temperature control system, shown in Figure 8, was capable of both heating and cooling the specimen to achieve the desired temperature profiles. Heating was provided by four quartz lamp heaters. These heaters were controlled by a microprocessor that used thermocouples for feedback control. The specimen was cooled by compressed air, regulated by both mechanical and computer controlled valves. The crack length was automatically monitored by the main computer through a D.C. electrical potential drop technique, and manually monitored with traveling telemicroscope with digital position readout.

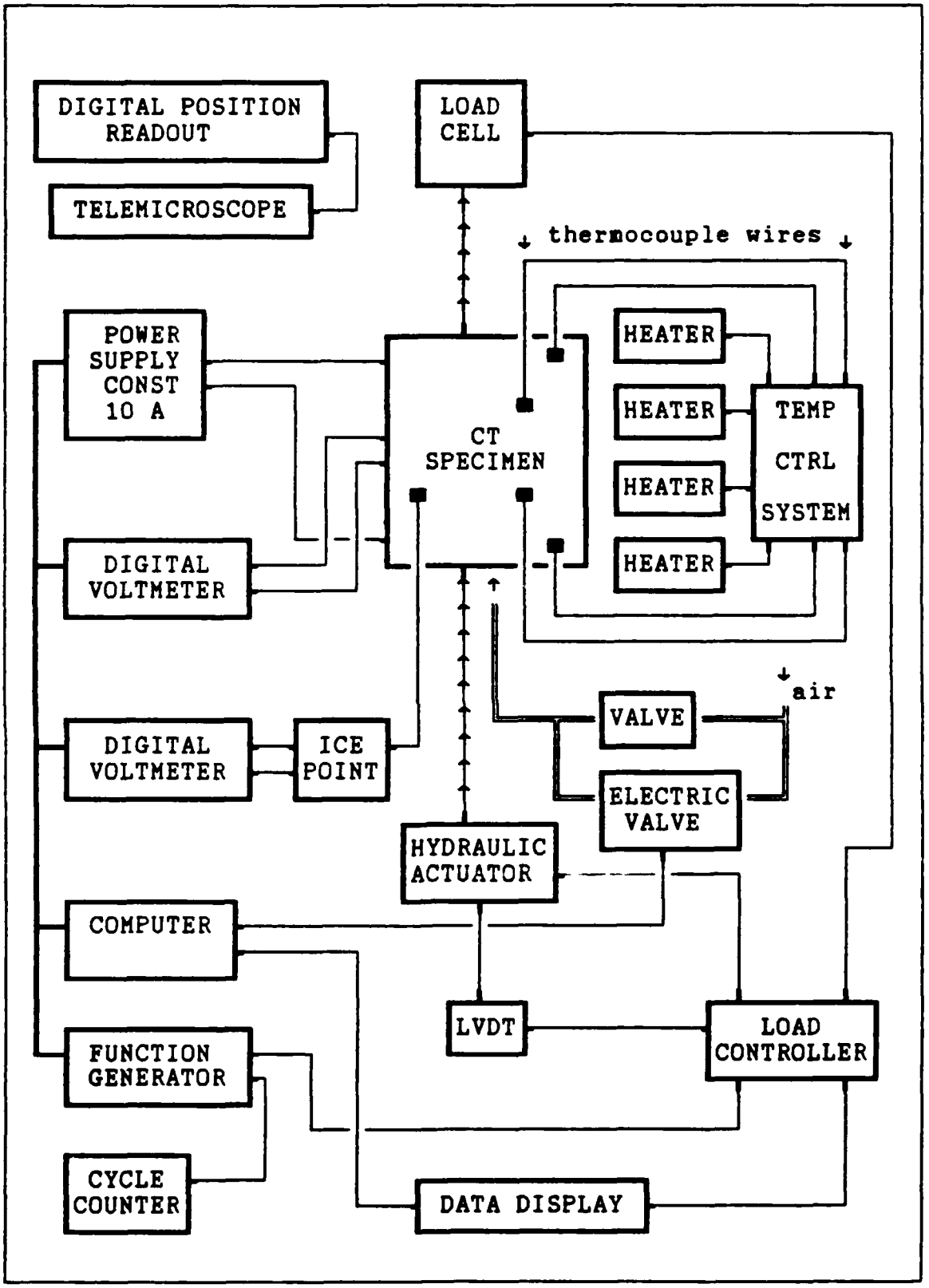

Fig. 6. Block Diagram of Testing System (5:22)

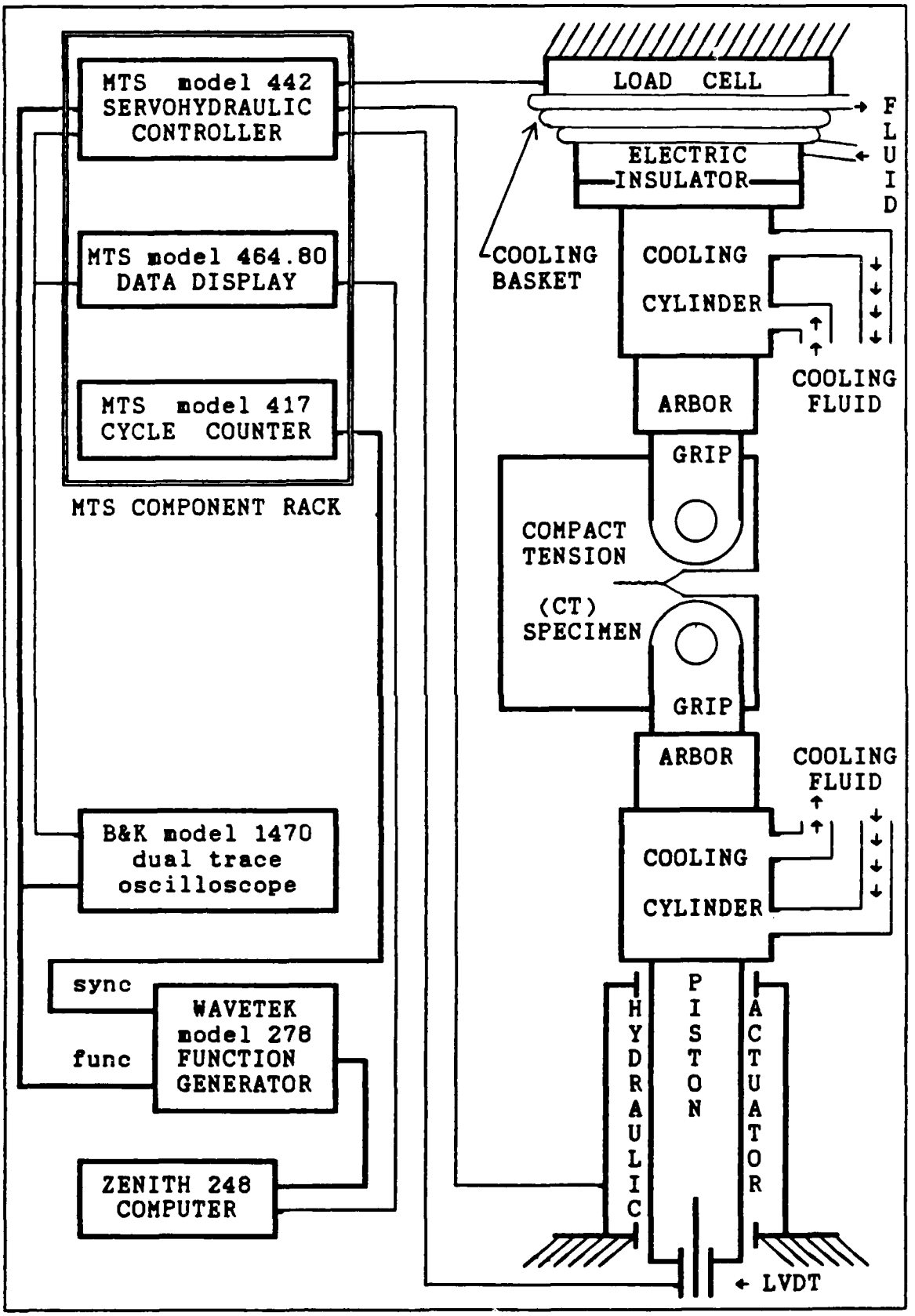

Fig. 7. Block Diagram of Mechanical Loading System (5:24)

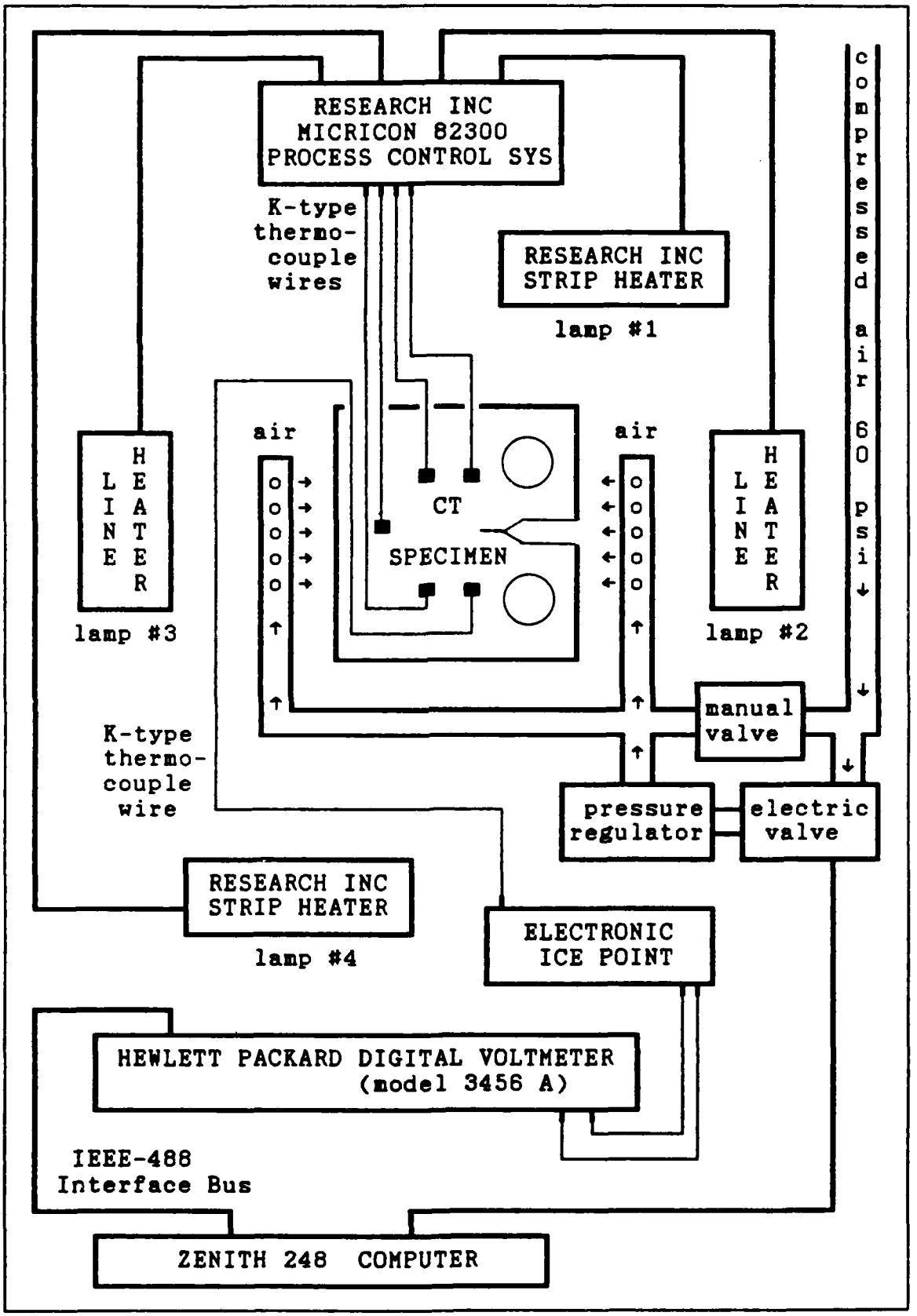

Fig. 8. Block Diagram of Temperature Control System (5:31)

Test Specimen

The compact tension specimen was used in this study. The specimen geometry is shown in Figure 9. The standards for the notch and all machining tolerances followed the ASTM Standard for Constant Amplitude Fatigue Crack Growth Rates Above 10^{-8} m/cycle E647 (25). The weight composition, heat treatment, and tensile properties of the Ti_3Al alloy are presented in Tables 1, 2, and 3 respectively.

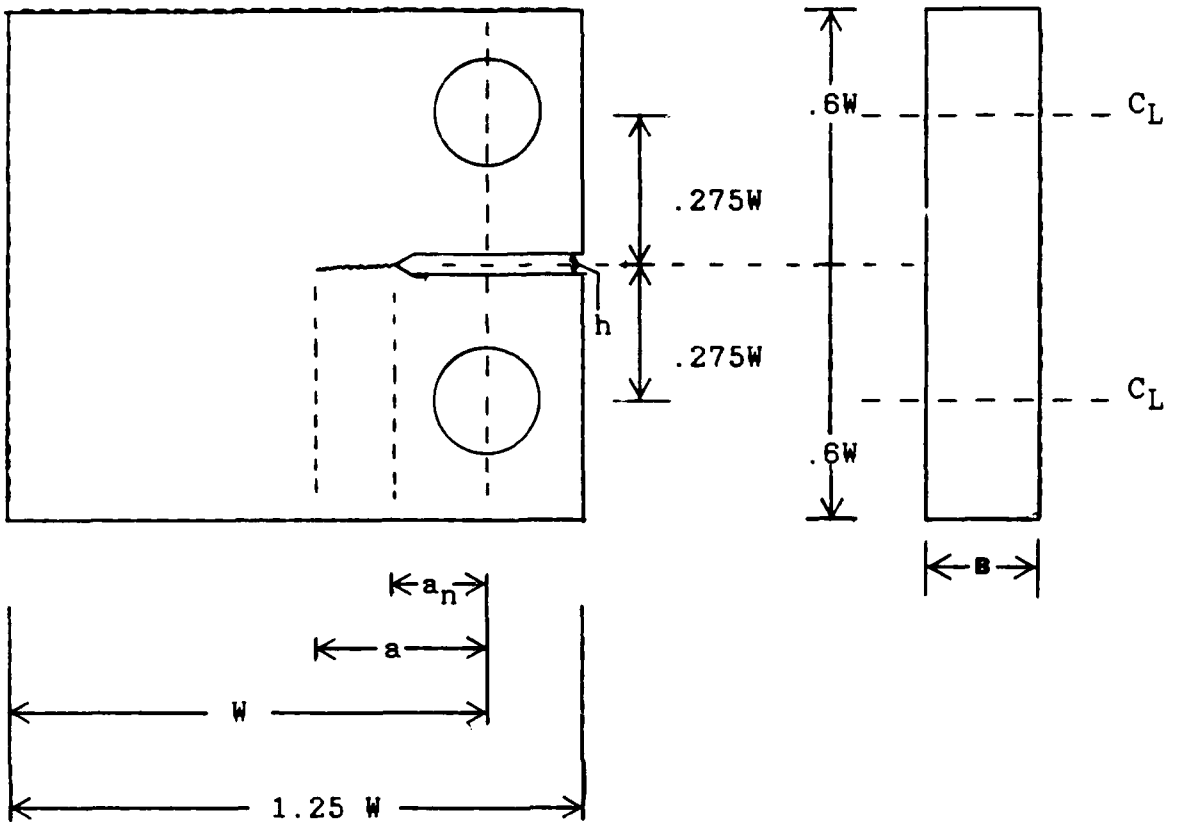

Specimen	W	B	a_n	h
88130	40.01	2.54	6.6	2.29
88133	40.01	2.29	6.6	2.29
88135	40.01	2.29	6.8	2.29
88136	40.01	2.29	6.9	2.29

All dimensions in millimeters

Fig. 9 Compact Tension Specimen Dimensions

Table 1 Weight Composition of the Ti_3Al Alloy

Element	Ti	Al	Nb	Fe	O	N
Weight %	Bal	13.50	21.40	0.080	0.0084	0.003

Table 2 Heat Treatment of the Ti_3Al Alloy

1 - 2100° F for one hour in vacuum

2 - Fan forced Argon cooled (3° F per second)

3 - Age harden at 1400° F for one hour in vacuum

4 - Air cool to room temperature

Table 3 Tensile Properties of the Ti_3Al Alloy

	25° C	300° C	650° C
UTS (Mpa)	669	707	504
0.2% YS (MPa)	555	412	337
Elong (%)	1.6	6.1	16.3
Young's Modulus (GPa)	91	86	55

Prior to testing two holes were drilled in the corners of each specimen as shown in Figure 10; these holes were used as connecting points for the DC current leads and through these leads a constant 10 amps was supplied to the specimen. The specimens were polished to a mirror finish to make visual crack measurement easier and more accurate. Eight type-K thermocouples and the electric potential pickup leads were then spot welded to the specimen; the location of these are given in Figures 11 and 10 respectively. Only four thermocouples were used at any one time, one thermocouple for each temperature zone in Figure 12. The other four were used as backups to the primary thermocouples.

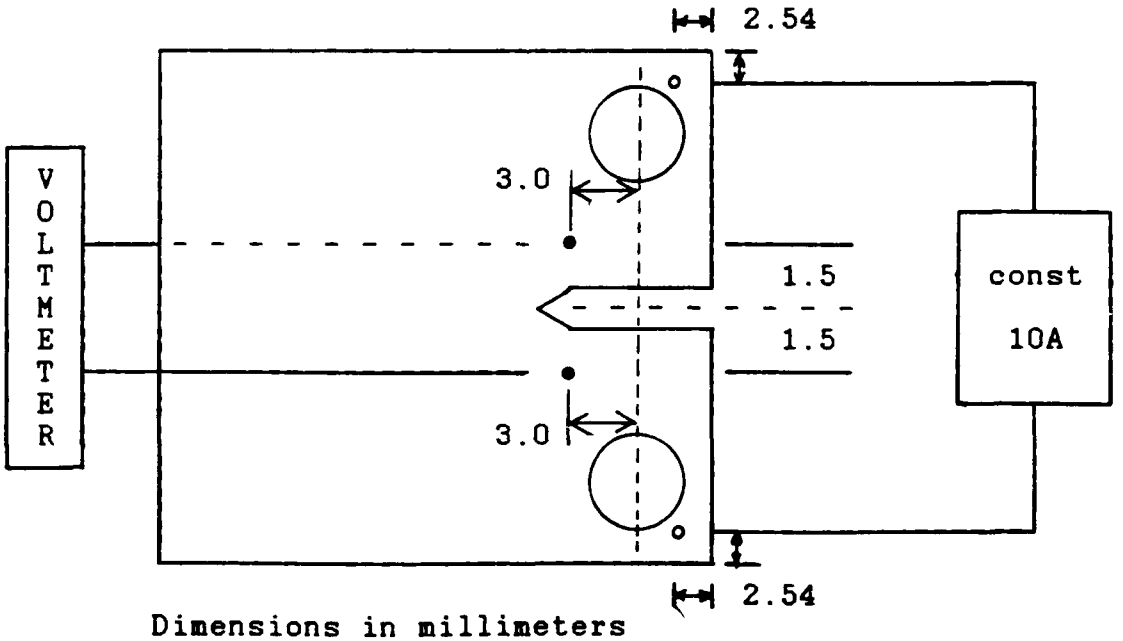

Fig. 10. D-C Current and Voltage Pick-up Locations

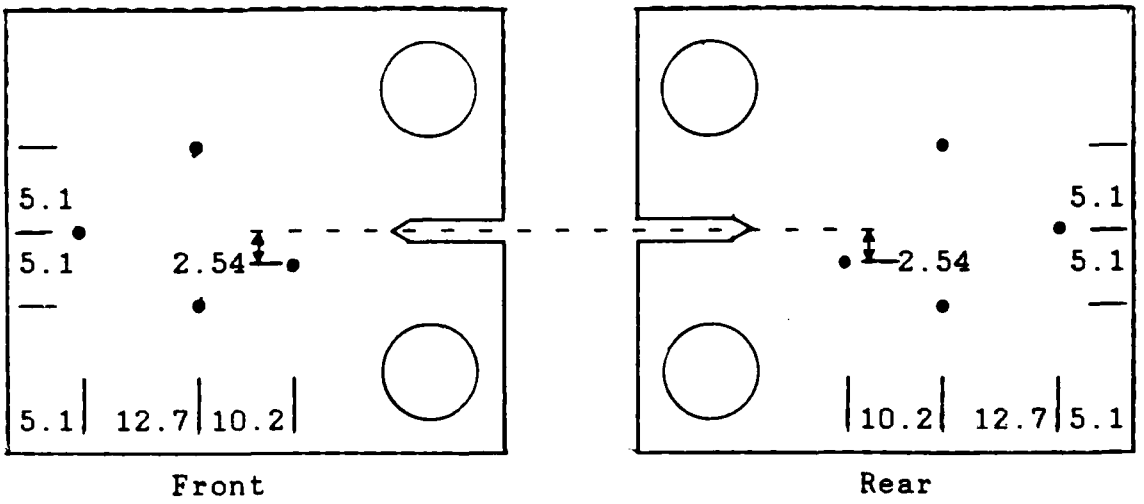

Fig. 11. Thermocouple Locations

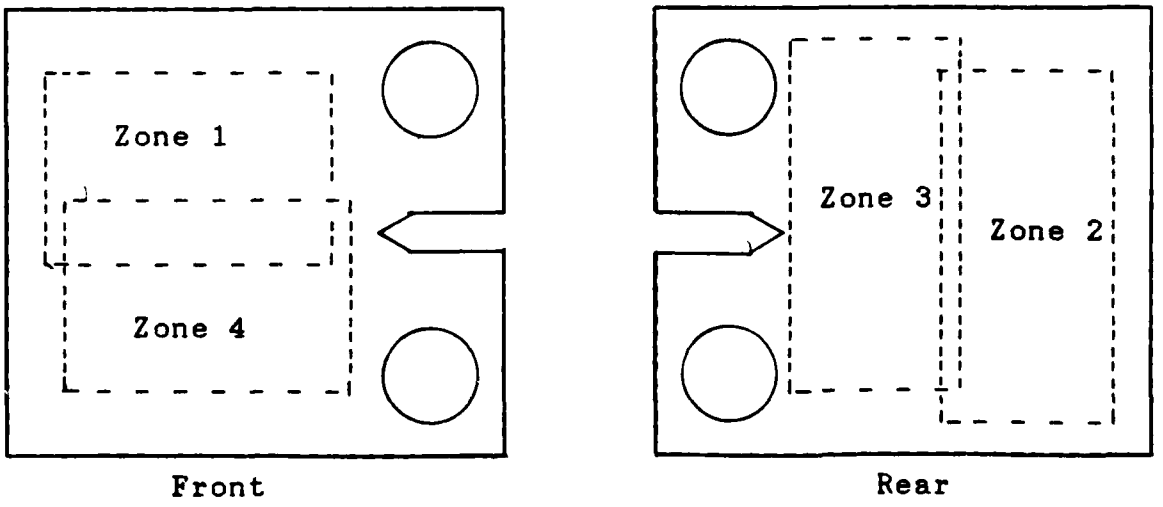

Fig. 12. Temperature Control Zones

Precracking

The specimen was then mounted into the MTS test frame for precracking. Precracking was performed according to ASTM standard E647 (25). The minimum fatigue precrack must be the larger of 0.1B, h, or 1.0 mm as shown in Figure 10. For these specimens, h was the largest (2.29 to 2.54 mm) and hence this value was used as the precrack length. The following equation was used to determine the load required for the desired values of the stress intensity range ΔK:

$$\Delta P = \frac{\Delta K \; B \; W^{1/2} \; (1-a/W)^{3/2}}{(2 + a/W)} \left[0.886 + 4.64 \frac{a}{W} - 13.32 \left[\frac{a}{W}\right]^2 + 14.72 \left[\frac{a}{W}\right]^3 - 5.6 \left[\frac{a}{W}\right]^4 \right]^{-1} \quad (8)$$

where

$\Delta P = P_{max} - P_{min}$

$\Delta K = K_{max} - K_{min}$

a = Crack length

W = Specimen width

All specimens were precracked to approximately 2.54 mm. The initial maximum intensity was approximately 12.0 MPa*sqr(m) and the final maximum intensity was approximately 8.1 MPa*sqr(m). This resulted in a final load of approximately 0.800 kN for each specimen. This final load was less than the 0.890 kN P_{max} used in the subsequent TMF tests. Figure 13 shows a typical load shedding during precracking. The precracking was computer controlled and the load was reduced in the following manner:

1.) The load was never reduced more than 20% at any one time.

2.) The crack was allowed to grow through three plastic zone sizes before the load was reduced.

3.) The plastic zone size was estimated by:

$$1/\pi(K'_{max}/\sigma_{ys})^2 \qquad (9)$$

where: K'_{max} was the terminal value of K_{max} from the previous load step

σ_{ys} was the yield strength of the specimen

Each specimen was precracked at the temperature at which the maximum load would occur during its subsequent test. The precracking fatigue frequency varied from 1 to 5 hz. Precracking for each specimen was started at 1 hz and was gradually increased to 5 hz after the voltage measurements indicated that crack growth was occurring. The computer monitored crack growth and reduced the load to meet the three criteria listed above. The precracking data are summarized in Table 4.

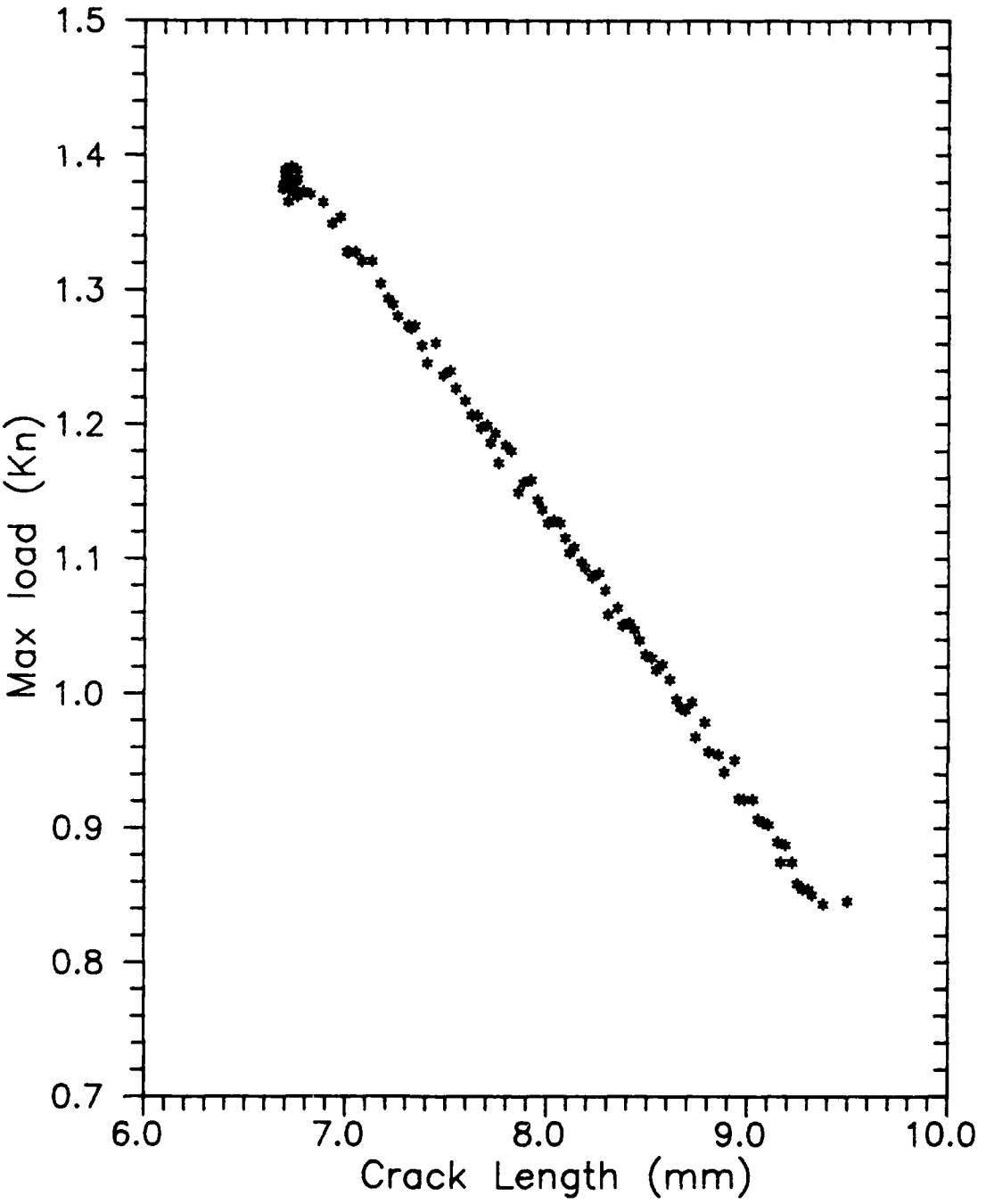

Fig. 13. Typical load shedding rate for precracking

Table 4 Precracking Summary

Specimen	Initial Values			Final Values			Temp. °C
	Crack (mm)	Load (kN)	K_{max}	Crack (mm)	Load (mm)	K_{max}	
88-130	6.6	3.56	26.9	10.1	.890	8.7	315
88-133	6.6	1.86	14.0	9.6	.826	7.8	482
88-135	6.8	1.38	11.7	9.9	.845	8.1	649
88-136	6.9	1.38	11.8	9.6	.824	7.8	649

Test Procedure

Several TMF tests were conducted using the test apparatus and instrumentation recently developed by Pernot (5). The test matrix is presented in Table 5. The test hardware developed by Pernot was used, but a computer program (MATE) developed by the University of Dayton Research Institute (UDRI) was used to control the test and acquire the test data. The program was designed to be flexible enough to allow for the following test parameters to be varied from test to test:

1.) Test specimen geometry

2.) Test load control (constant P_{max}, constant K_{max}, Decreasing P_{max} precracking, etc.)

3.) Test temperature limits

4.) Load/Temperature phase difference

5.) Cycle time

Table 5 Test Matrix

Specimen	Test Type*	Temp. Range (°C)	Cycle Time (seconds)
88130	III	315-649	96
88133	IV	315-649	96
88135	V	649	144
88136	VI	315-649	144

* - See Figure 14 for details

All tests were conducted using a constant maximum load of 0.89 kN and a load ratio of 0.1. The test temperature and load/temperature phase varied from test to test. Figure 14 shows the load/temperature relationships for the various tests conducted and analyzed in this investigation. This figure will be referred to throughout the text to clarify the crack growth analysis. The load/temperature phase angle was defined as the angle that the temperature lags the load in a 360 degree cycle. This relationship is shown in Figure 15.

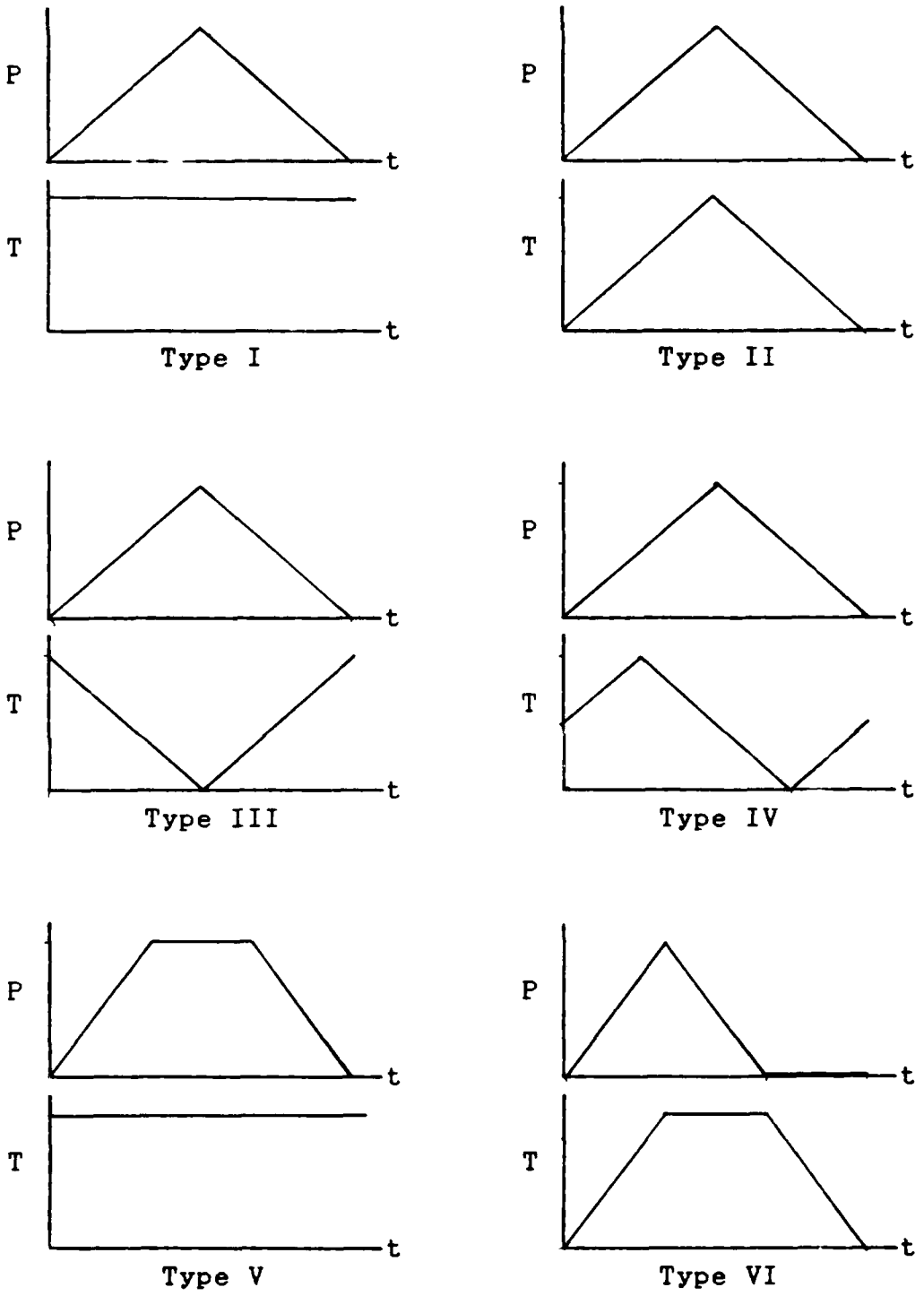

Fig. 14. Load (P) and Temperature (T) Profile Types

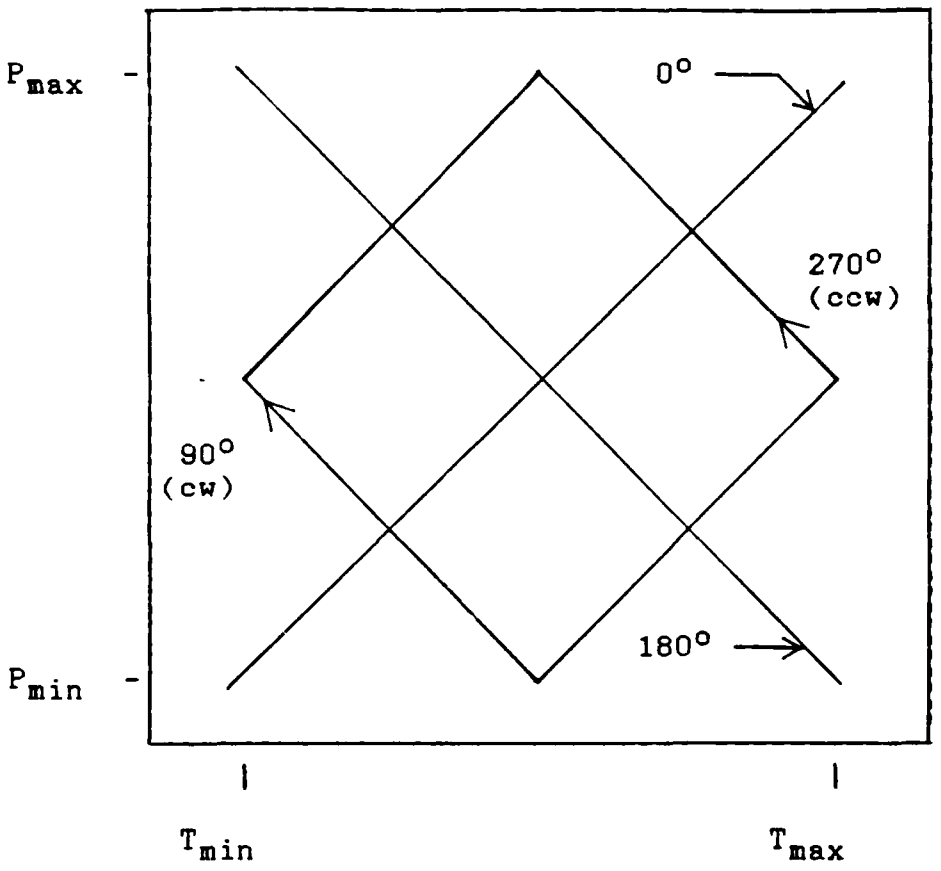

Fig. 15 Temperature/Load Phase Angles

The basic test procedure was the same for all tests. Data was input into the MATE program to define each test. This data included initial crack length, maximum load, maximum and minimum temperature, phase angle, etc. During this initialization process the temperature and load profile information was sent to the Micricon and MTS controllers respectively. The power supply and voltmeter were also initialized at this point.

While the test was running, the Micricon used feedback from the four thermocouples (one for each zone) to maintain the proper temperature profile. Each zone was controlled independently, using one quartz lamp to heat each zone. A small amount of compressed air was blown over the specimen during the heating portion of the cycle; this was found to provide a more uniform temperature through the entire specimen. Compressed air, as shown in Figure 8, was blown at a much more rapid rate during the cooling portion of the cycle to maintain a uniform temperature through the specimen. The closed loop heating and cooling system was able to heat and cool the crack-tip region of the specimen at a rate of 7^{o} C per second, while maintaining a temperature over the specimen within one to three percent of the desired temperature at any instant in time. Figure 16 shows a typical temperature profile.

The crack length of the specimen was automatically measured using a D.C. potential drop technique. A direct current of constant 10 amps was passed through the specimen. The voltage was measured using the voltmeter leads previously placed on the specimen. With increased crack length, the uncracked cross-sectional area of the test specimen decreased, its electrical resistance increased, and the voltage difference between the two leads spanning the crack increased. This voltage was converted to crack length by the MATE program using a closed form empirical solution for

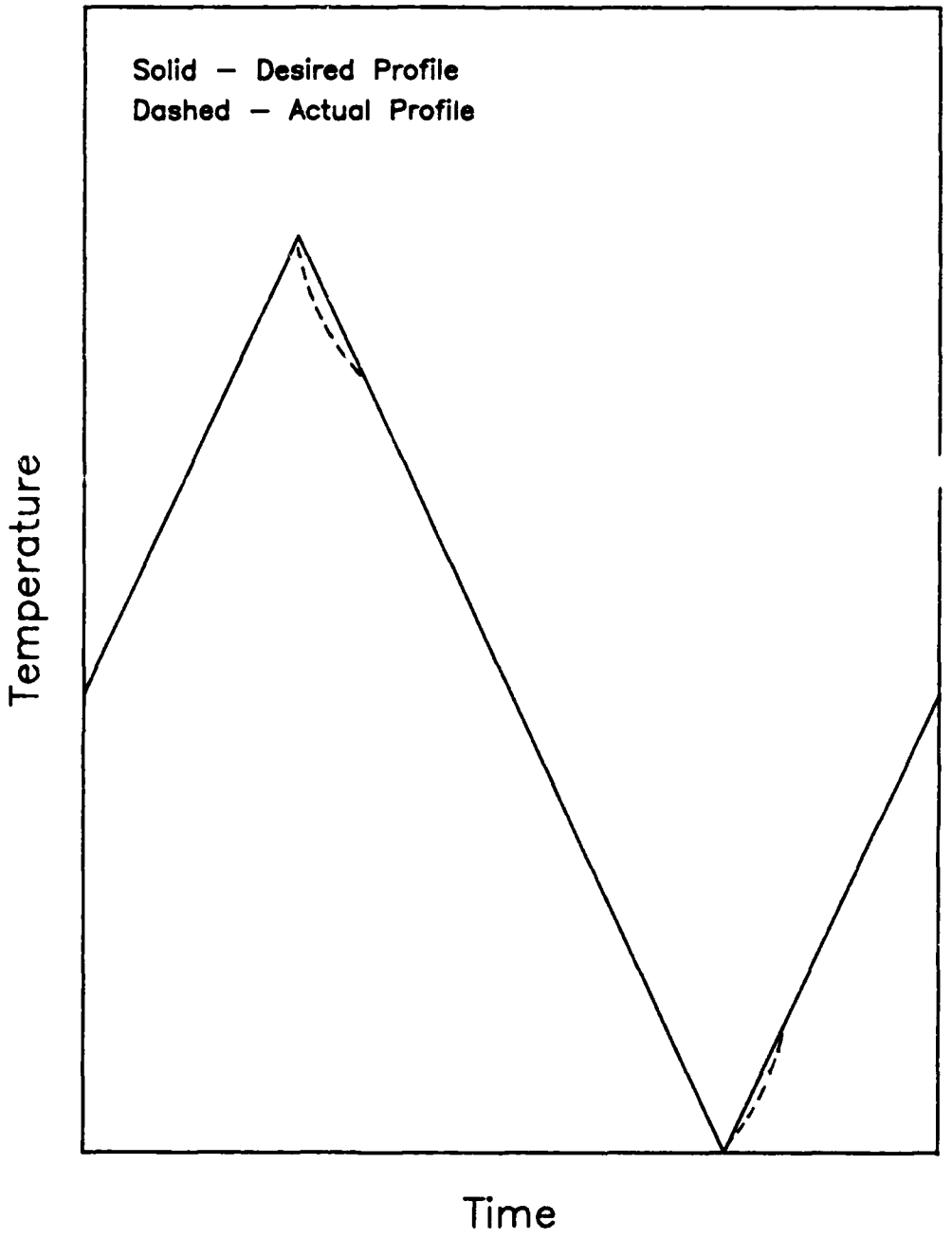

Fig. 16. Typical TMF Temperature Profile

the electrical potential field in a compact tension specimen by Johnson (26:442-445). This method was previously found to produce crack length data accurate to within ± 0.1 mm under similar conditions (27:111).

Three factors have been identified by Hartman and Johnson (27:106) as significant contributors to errors in crack length measurement using the D.C. potential technique. They are material resistivity effects, thermal emf effects, and fracture surface bridging effects. Material resistivity is generally a function of temperature. Prior to the start of each test, a data acquisition point was chosen in the fatigue cycle. Every subsequent voltage measurement was taken at that same point in the cycle. Therefore, within each TMF test all crack length voltage readings were taken at the same temperature, thus minimizing any resistivity error.

Thermal emf voltages are generated whenever two junctions of dissimilar metals are held at different temperatures. Since the voltmeter leads are made of a different material than the specimen, a thermoelectric voltage was generated at the temperature range of these tests. These lead wires were positioned to reduce the temperature difference between the two junctions, however some thermal emf did exist. To eliminate this error, the voltage was first taken with the 10 amp power supply on, then the power supply was turned off and the thermal emf was recorded. The thermal

emf was then subtracted from (or added to) the first voltage reading to obtain a corrected voltage for use in the crack length calculation. This method produced voltage data which was relatively independent of thermal emf.

Fracture surface bridging changes the effective surface area through which the current flows. Any such change, (ie. an increase in the conducting path) will reduce the measured voltage and cause errors in the calculated crack length. If at any time during the cycle the applied load becomes less than or equal to the closure load, the crack surfaces will come in contact. This effect is further complicated by oxide formation on the fracture surfaces. The oxides provide an insulating layer between the fracture surfaces which will also alter the measured voltage. These oxides will partially eliminate the voltage errors due to closure, but their behavior in terms of the amount of oxide present and its insulating capability is very hard to quantify. To eliminate any closure effects in these tests, the voltage was measured very near the maximum load as shown in Figure 17; this ensured that the crack was fully opened when the voltage was taken.

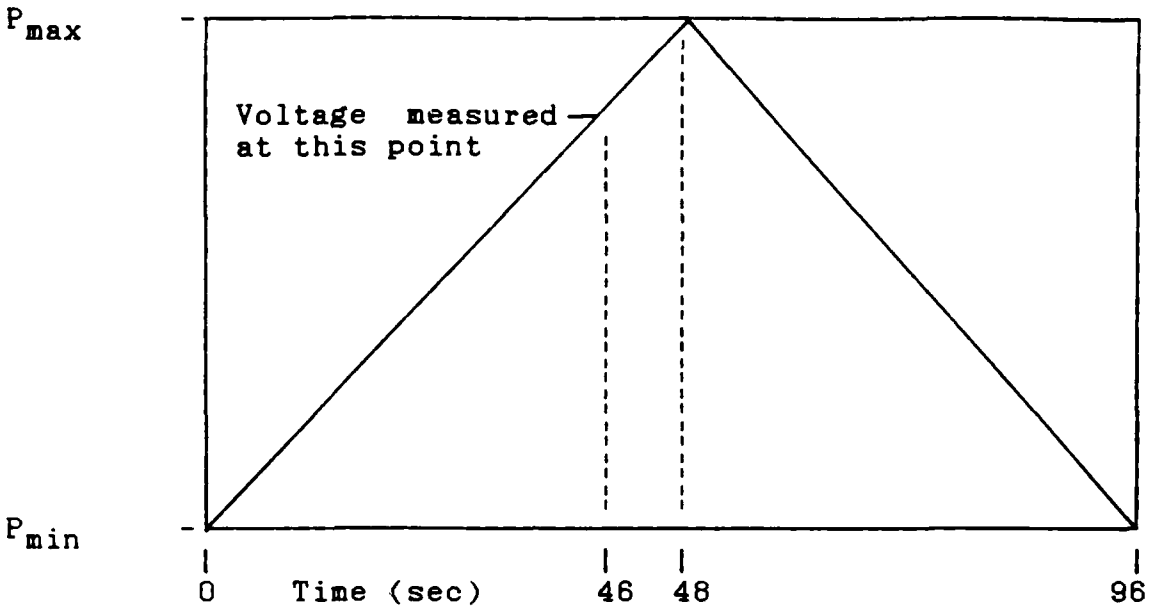

Fig. 17 EP Voltage Data Point for all Tests.

In order to verify the crack length data obtained by the MATE program, optical measurements were made with a 0.0013 mm resolution Gaertner telemicroscope and digital position read-out system. The crack measurement systems are shown in Figure 18. A reference mark was inscribed on each specimen behind the notch; this mark was found to provide more consistent optical crack length readings than using the notch as a reference. A comparison of the two crack measurement methods is presented in Figure 19.

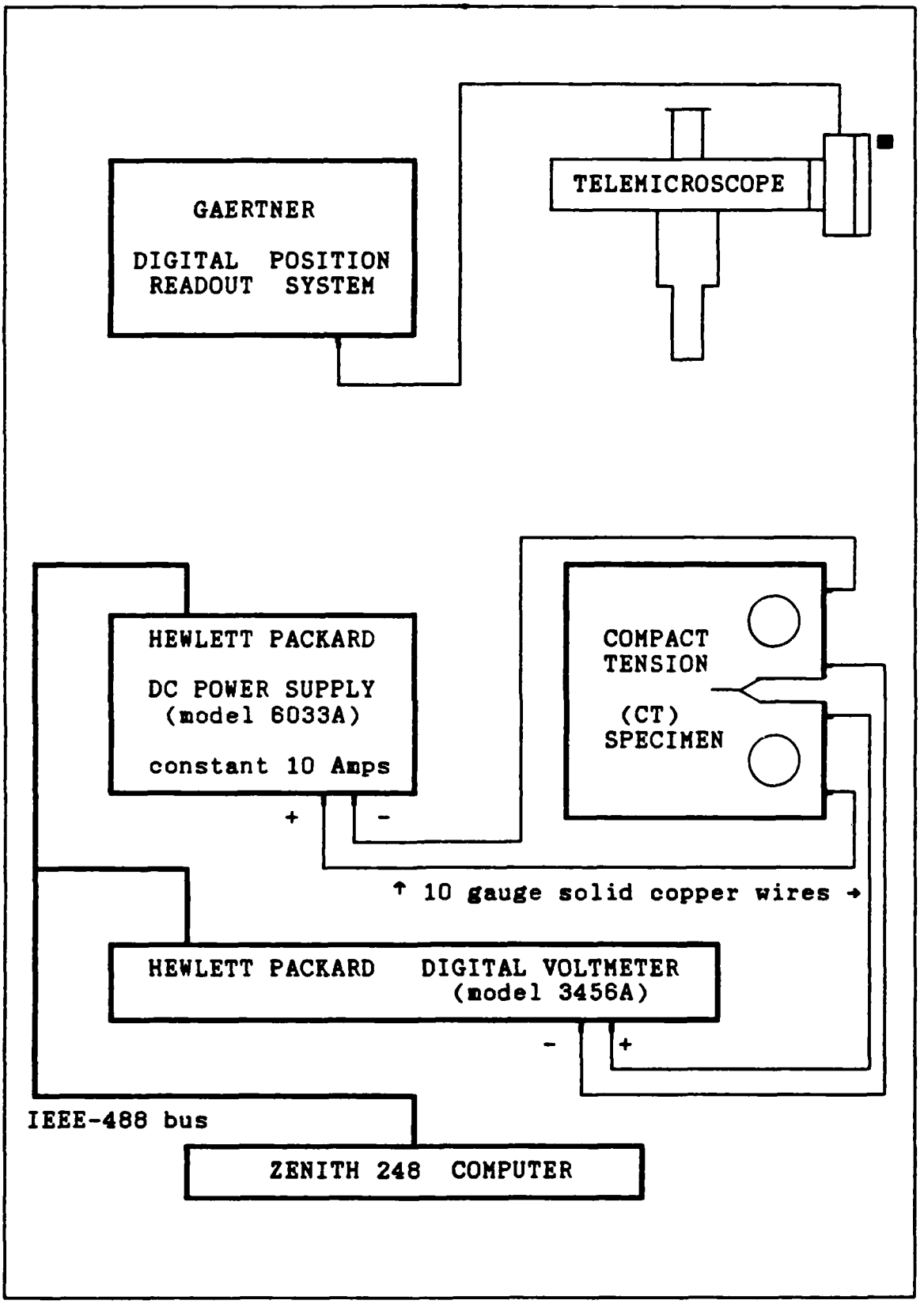

Fig. 18. Crack Length Measuring Devices (5:44)

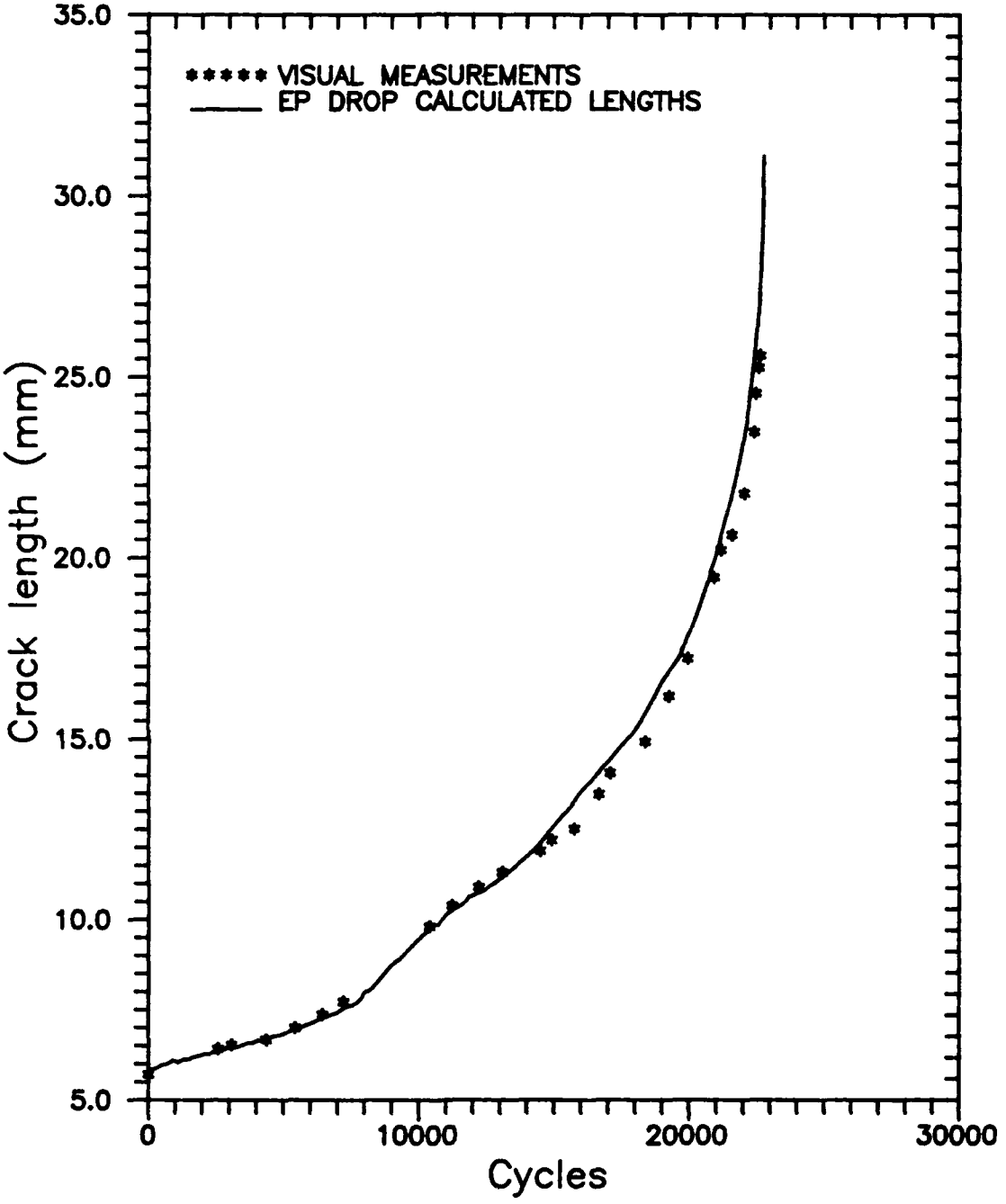

Fig. 19 Comparison of Visual and EP Crack Lengths

IV. Data Reduction

As described previously, crack length measurements were taken via electrical potential drop by the controlling microcomputer. Each of these crack lengths was stored in computer memory along with corresponding load and cycle count. Therefore, the major effort in data reduction was to reduce this crack length vs. cycle count (a vs. N) data to a da/dN vs. ΔK form. This would allow for the comparison of crack growth rates between the various tests. The procedure used in this data reduction is described below.

The crack length was measured every hour during each test. This interval was reduced to every 20 or 30 minutes in the later stages of a test to capture the accelerated crack growth data. The reason for this was that any malfunction in the test system, such as a burned out quartz heating lamp or loss of cooling air, would disrupt the electric field on the specimen. This change in the potential field would cause the D.C. voltage, and subsequent calculated crack length, to be in error. Taking crack length measurements this often provided more data points than were needed and allowed for the deletion of any erroneous points. However, the crack growth between readings was sometimes as small as 0.002 mm, especially during the early part of a test. This amount of growth was far less than the precision of the measurement system, and caused fluctuations

in the da/dN vs. ΔK data when the standard seven point incremental polynomial technique was used to reduce the crack growth data (a vs. N). This technique is outlined in ASTM Test for Constant Load-Amplitude Fatigue Growth Rates Above 10^{-8} m/cycle E647 (25).

One option available to reduce the error in the da/dN vs. ΔK data would have been to edit the a vs. N data so that the Δa between successive data points was at least ten times the crack length measurement precision (25). This would have required elimination of much of the a vs. N data. In order to reduce, the error and also include all available crack growth data, an alternative method was used. This method was developed by Larsen (28:226-238), and was a modification of the ASTM incremental method. This method is shown schematically in Figure 20. Figure 21 shows a comparison of da/dN vs. ΔK data using the standard ASTM method and the modified method.

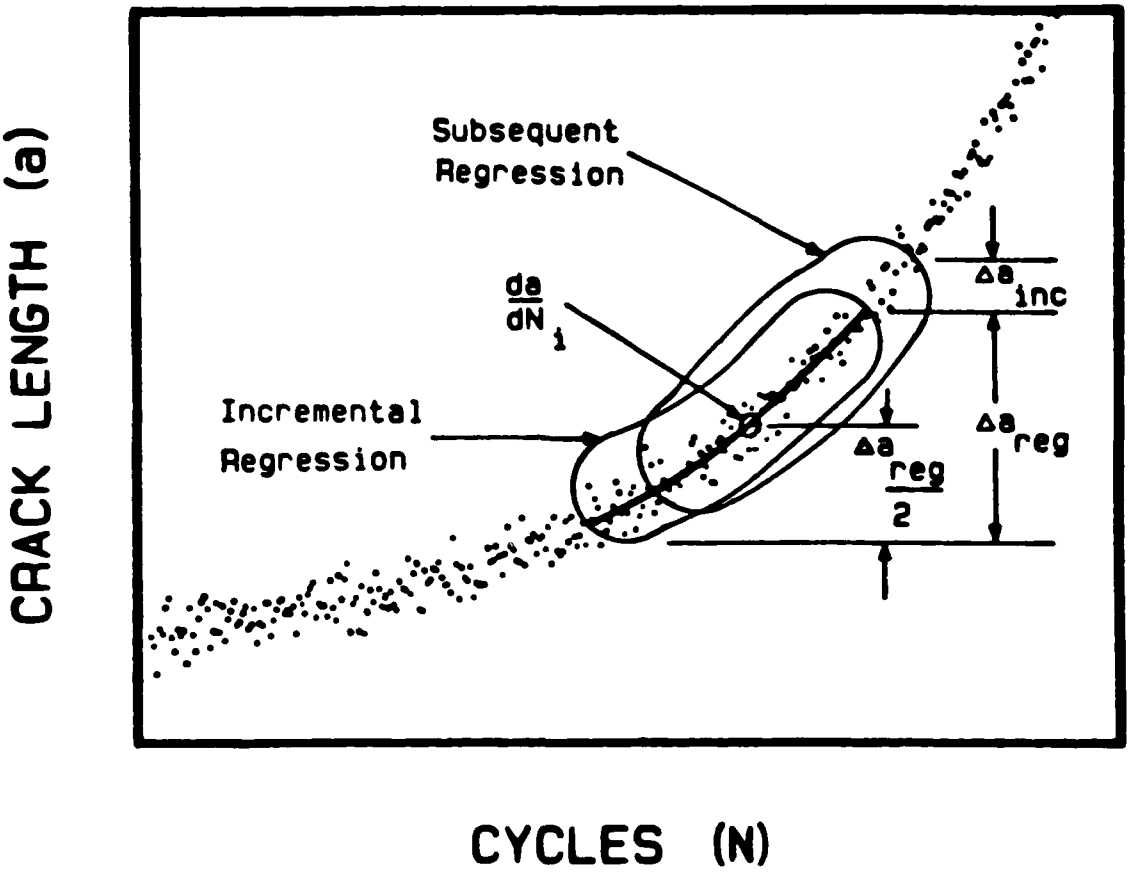

Fig. 20 Schematic of the Modified Polynomial Technique for Reduction of Fatigue Crack Growth Data (28:237)

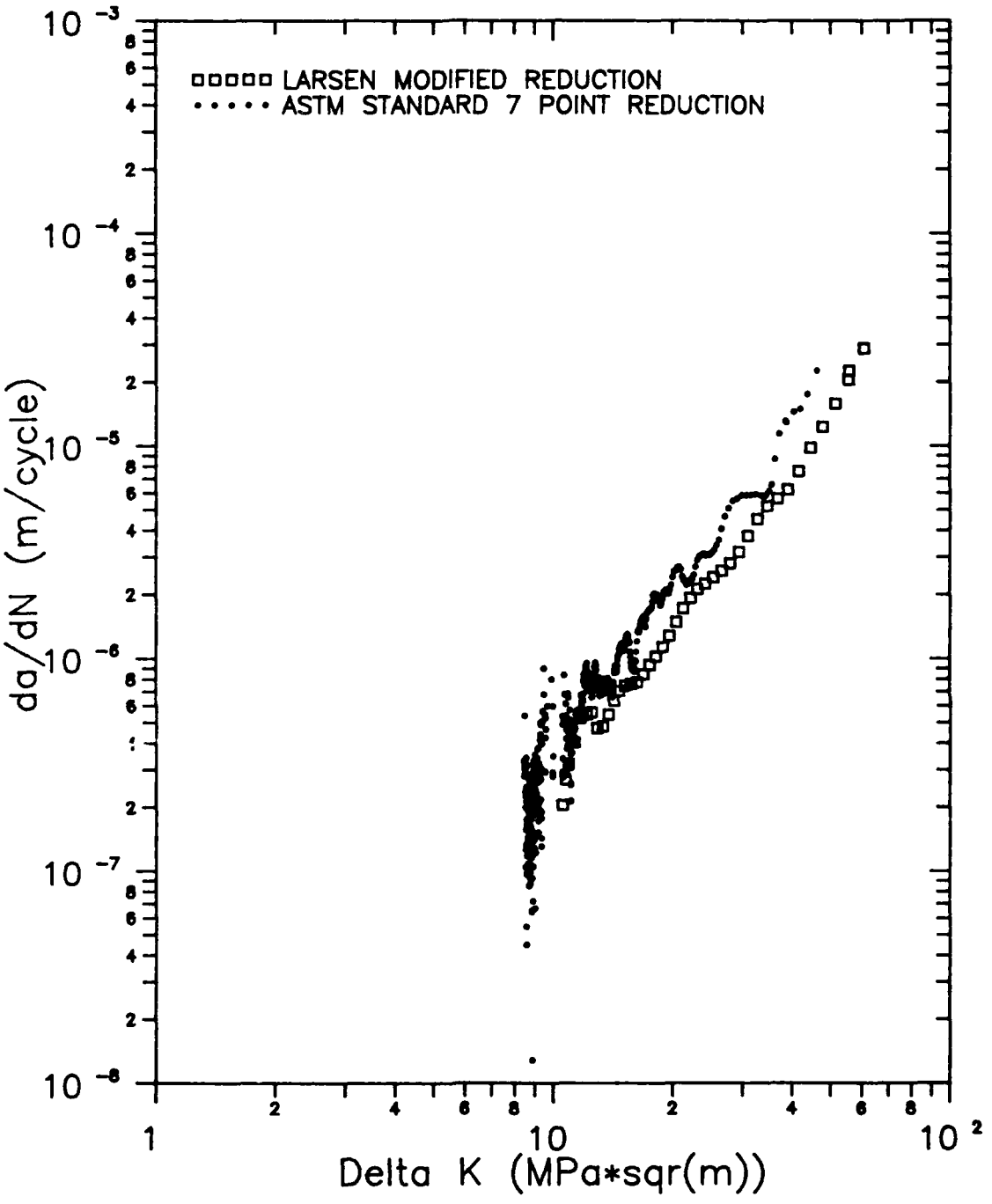

Fig. 21. Comparison of Larsen Modified and Standard ASTM Incremental Polynomial Results

This modified method differs from the ASTM standard by the choice of data which is used in each incremental regression. In the ASTM method, a preselected number of data points, usually seven, is used in each regression; the number of data points used is the same for all regressions. In this modified method the number of data points used in the regressions is chosen in two different ways. During periods of slow crack growth, all crack length data in the interval Δa_{reg} were fitted with the second degree polynomial. As many as 200 (a,N) data points were in the first Δa_{reg} interval and were used in the first regression. For each interval the regression was performed and ΔK_i and da/dN_i was calculated at the midpoint of the interval. The interval would "slide" up the a vs. N curve by an amount Δa_{inc} and another regression was performed. The number of (a,N) data points contained in the Δa_{reg} interval decreased with each subsequent regression due to the increasing slope of the a vs. N curve. If there was a point in the a vs. N curve where there were less than seven data points in the Δa_{reg} interval, the program would revert to the standard incremental polynomial technique using seven data points. Therefore, the standard seven point solution was obtained whenever there was a gap in the a vs. N data, or when the crack growth between readings was larger, such as the upper portion of the a vs. N curve.

For the data presented here Δa_{inc} was set to 0.508mm, and Δa_{reg} was set to 6 times Δa_{inc}. These values provided good data reduction for the a vs. N data collected in the tests. The value chosen for Δa_{reg} was approximately five times the precision of the measurement system. This method provided a means to reduce a vs. N data, in a typical test, from as many as 650 data points to 40 or 50 da/dN vs. ΔK data points, without the fluctuation which can result from the standard incremental polynomial technique.

V. Results and Discussion

Test Sequence

The purpose of this present investigation was to perform several baseline TMF tests of the Ti_3Al alloy, which could provide the necessary data to develop a fatigue crack growth prediction model for this material under general TMF conditions. Prior to the start of this effort, a 649° C isothermal fatigue test and a 315-649° in-phase (IP) TMF (type II in Figure 14) test were conducted by Pernot (5). Also a 315° isothermal fatigue test had been conducted by the Air Force Materials Laboratory. All three tests were conducted at .01 hz with a load ratio of 0.1.

The first test conducted during this present study was a 180° phase (OP) TMF test (type III in Figure 14). A 270° phase TMF test (type IV in Figure 14) was then conducted. Both of these TMF tests were conducted over a temperature range of 315-649° C. During the time these tests were being conducted, sustained load crack growth tests of this same alloy were being conducted by Staubs (29). The impact of these sustained load tests on the present investigation is explained below.

As mentioned previously, the linear cumulative damage model developed by Heil (2) was considered as a model for use with this Ti_3Al alloy. The sustained load tests by Staubs (29) showed no crack growth in this alloy at 649° C.

Heil's model obtained the time-dependent damage contribution by integrating the sustained load crack growth rate over the loading portion of the cycle. Hence, this model would predict no time-dependent contribution for damage in the Ti_3Al alloy. However the .01 hz isothermal fatigue and TMF tests indicated that time-dependent damage is present. It was thus obvious that a simple linear summation model such as Heil's might not be applicable to this material. Other damage mechanisms were then investigated to provide a clearer picture of how the Ti_3Al alloy behaves under fatigue and sustained load at 649° C. Therefore, two tests were conducted to investigate the time-dependent damage in this material at 649° C. The first test was a 649° C isothermal fatigue test with a 48 second hold time at P_{max}, as shown in Figure 22. The second test was an in-phase TMF test with a 48 second hold time at T_{max}; its profile is presented in Figure 23.

Crack growth data, from all eight TMF and isothermal fatigue tests, were analyzed to determine the various types of damage mechanisms present in this alloy. These test are summarized in Table 6. Complete discussion on each of these tests is presented in the following section.

Table 6 Summary of Tests Analyzed

Specimen	Test Type[1]	Cycle Time (Seconds)	Temp. Range (°C)	Load Ratio
88129*	I	96	649	0.1
88131*	II	96	315-649	0.1
88134**	I	96	315	0.1
88130	III	96	315-649	0.1
88133	IV	96	315-649	0.1
88135	V	144	649	0.1
88136	VI	144	315-649	0.1
88142**	I	0.2	649	0.1

* Indicates test performed by Pernot (5)

** Indicates test performed by USAF Materials Laboratory

1 See Figure 14 for details

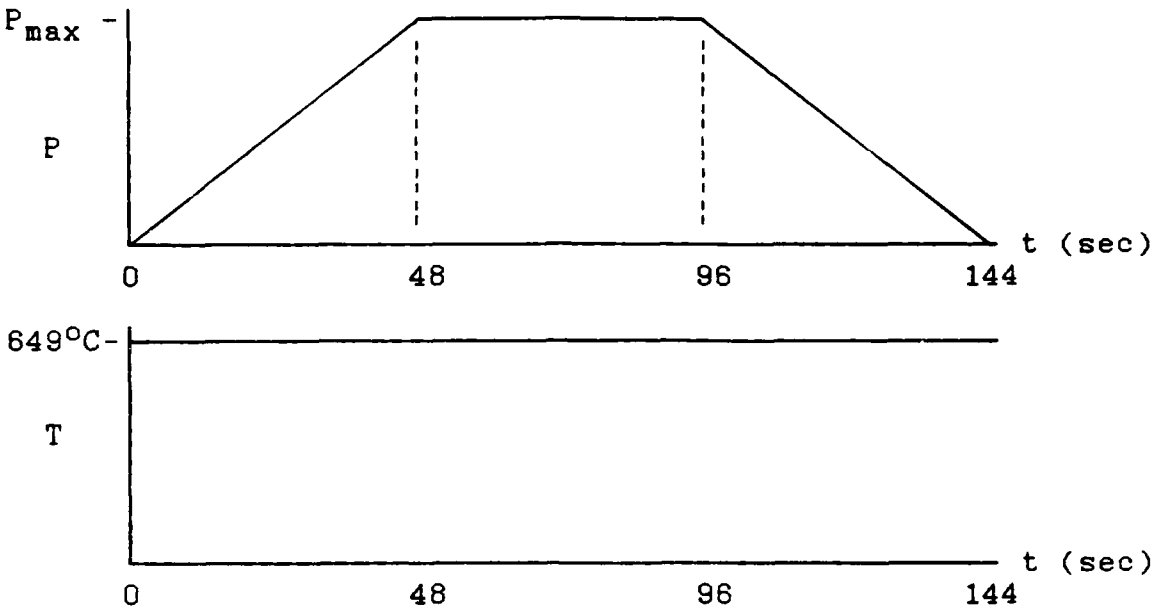

Fig. 22. Load (P) and Temperature (T) Profiles for Test with Hold Time at P_{max} (Type V)

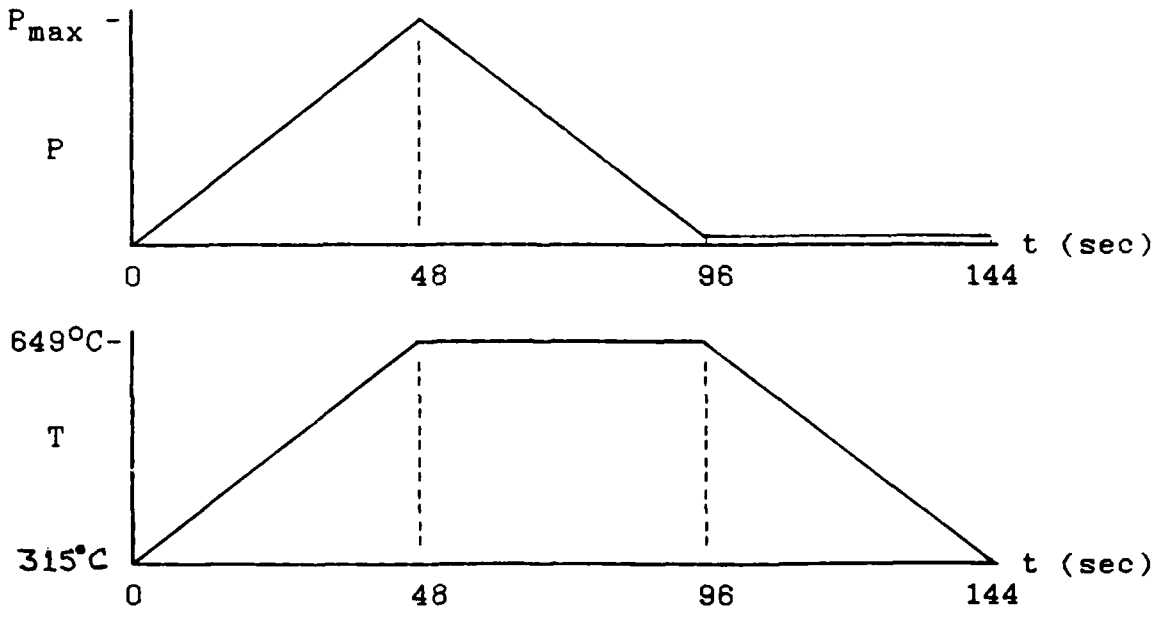

Fig. 23. Load (P) and Temperature (T) Profiles for Test with Hold Time at T_{max} (Type VI)

Fatigue Crack Growth Analysis

Examination of the crack growth data from all eight tests analyzed indicated that the data fell into region II of the crack growth curve in Figure 5. Therefore, all the data were fitted to the Paris equation . The coefficients for the Paris equation are presented in Table 7. The n values represent the slope, and the C values represent the y-axis intercept of the da/dN vs. ΔK curve. Very little scatter was found in the slope between these tests, except for the 315° C isothermal test. For these seven tests the slopes ranged from 2.55 for the 649° C isothermal fatigue test (.01 hz), to 3.11 for the 649° C isothermal fatigue test with hold time. For these seven tests, the intercepts ranged from 4.75E-10 for the 270° phase TMF test, to 6.66E-9 for the 649° C isothermal fatigue test (.01 hz). As noted above the 315° C isothermal fatigue test had substantially different values for C and n. Also, the 315° C isothermal fatigue test data showed a period of fluctuation, in da/dN, for Δk values of approximately 10 MPa*sqr(m). This fluctuation may have been due to transient crack growth behavior, which is sometimes seen when a specimen is precracked at a temperature different from its subsequent test temperature. This fluctuation could also have been caused by the data reduction technique, as described in section IV of this thesis. Since the cause of this fluctuation could not be determined, this fluctuating data

were not used to determine the Paris coefficients for this test. Figures 24 through 31 show these experimental crack growth data for all eight tests, along with the fitted Paris equation for each test.

Table 7 Paris Equation Coefficients

Specimen	C	n
88129	3.45E-09	2.92
88130	8.29E-10	2.48
88131	6.66E-09	2.55
88133	4.75E-10	2.92
88134	3.29E-13	4.50
88135	6.72E-10	3.11
88136	2.12E-09	2.71
88142	6.45E-10	2.64

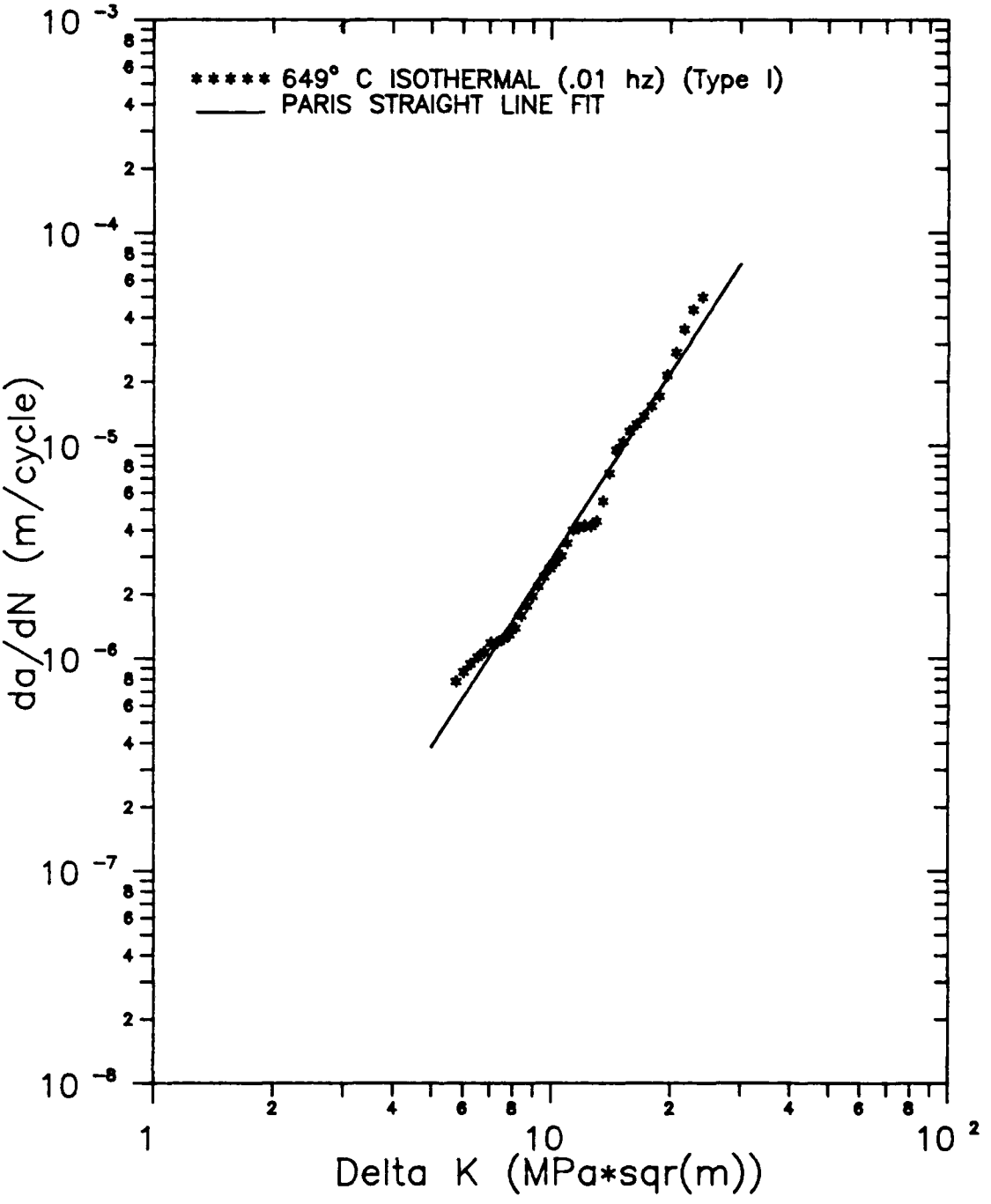

Fig. 24. 649° C Isothermal (.01hz) crack growth data with straight line fit

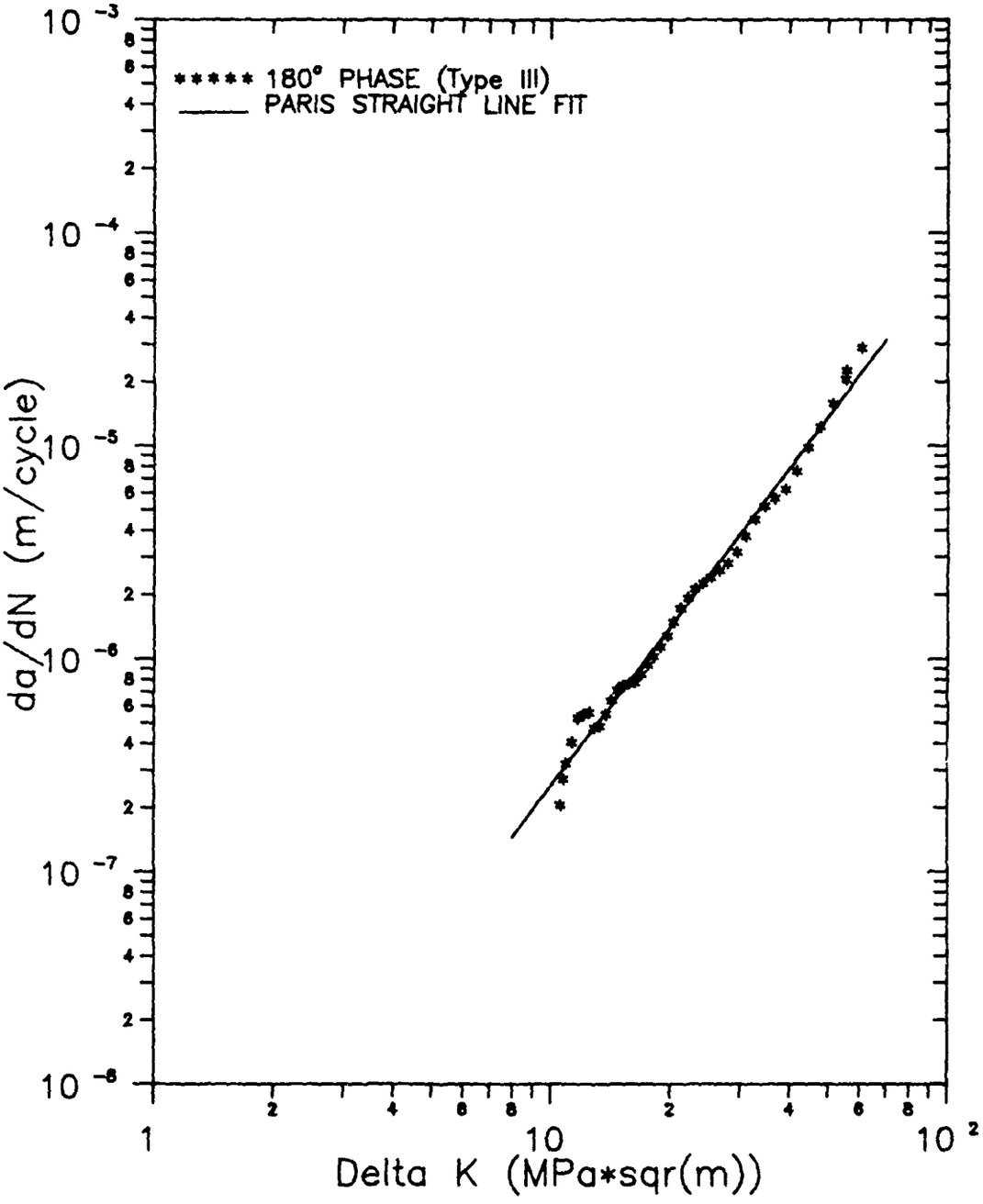

Fig. 25. 180° phase (OP) crack growth data with straight line fit

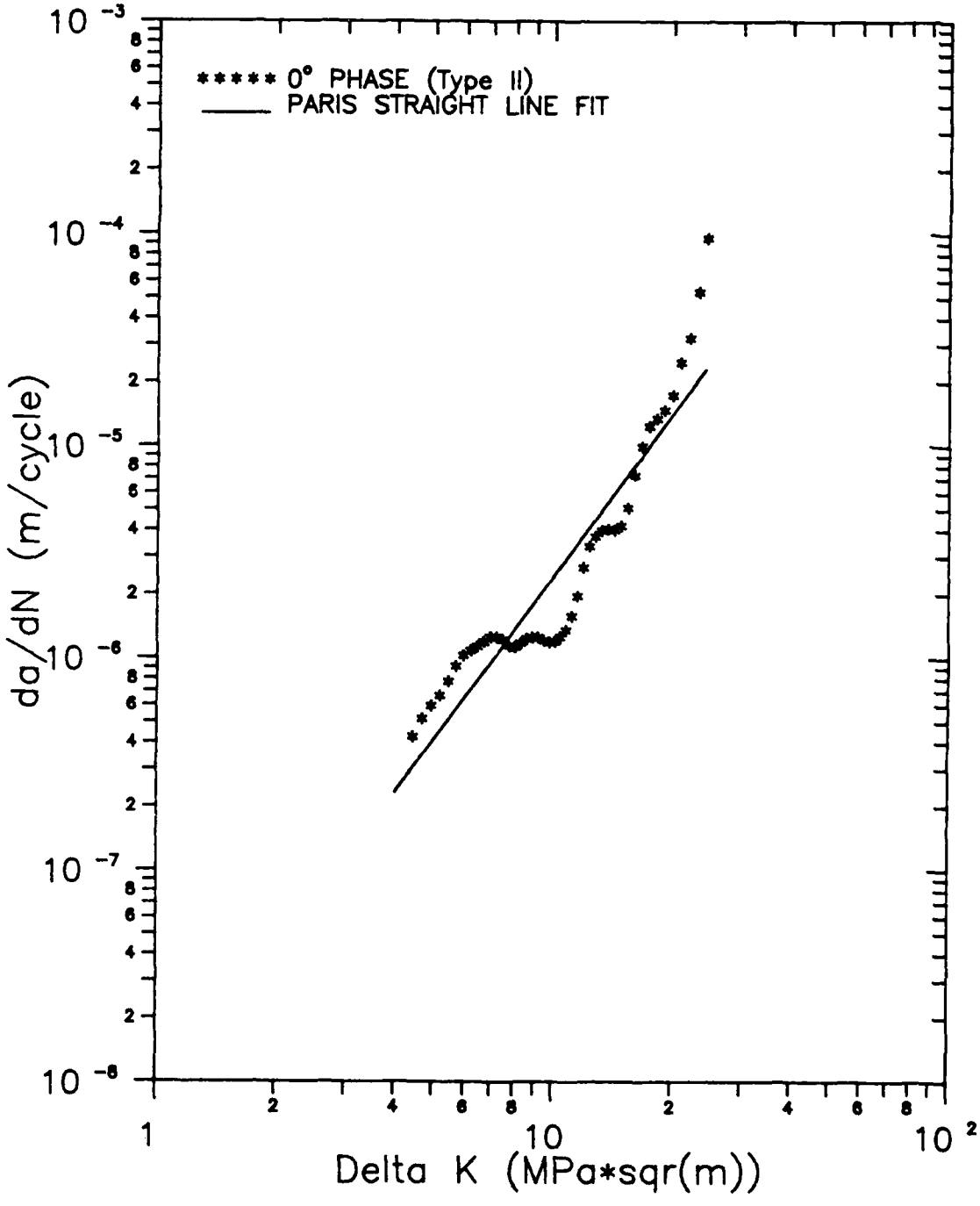

Fig. 26. In phase crack growth data with straight line fit

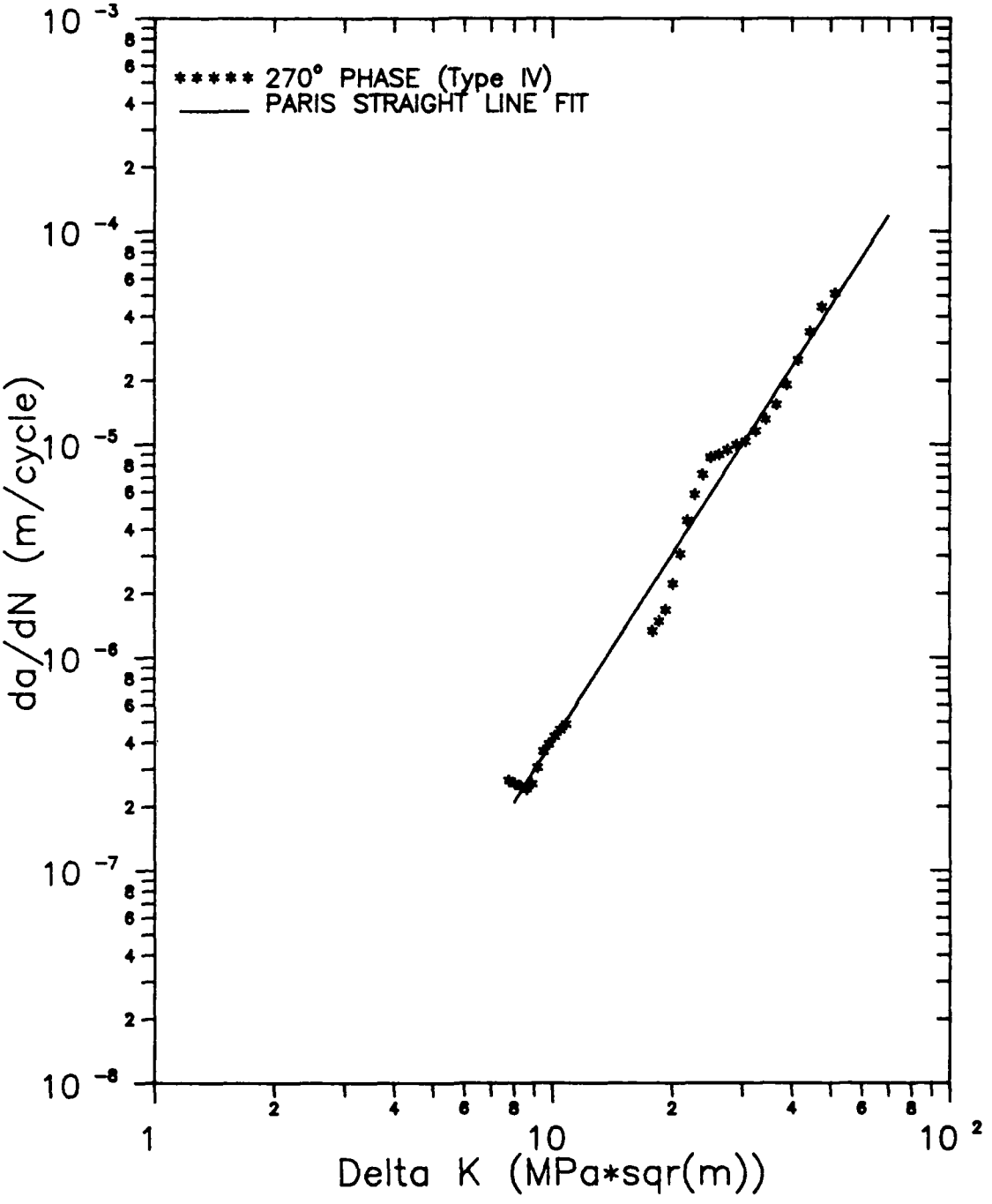

Fig. 27. 270° phase crack growth data with straight line fit

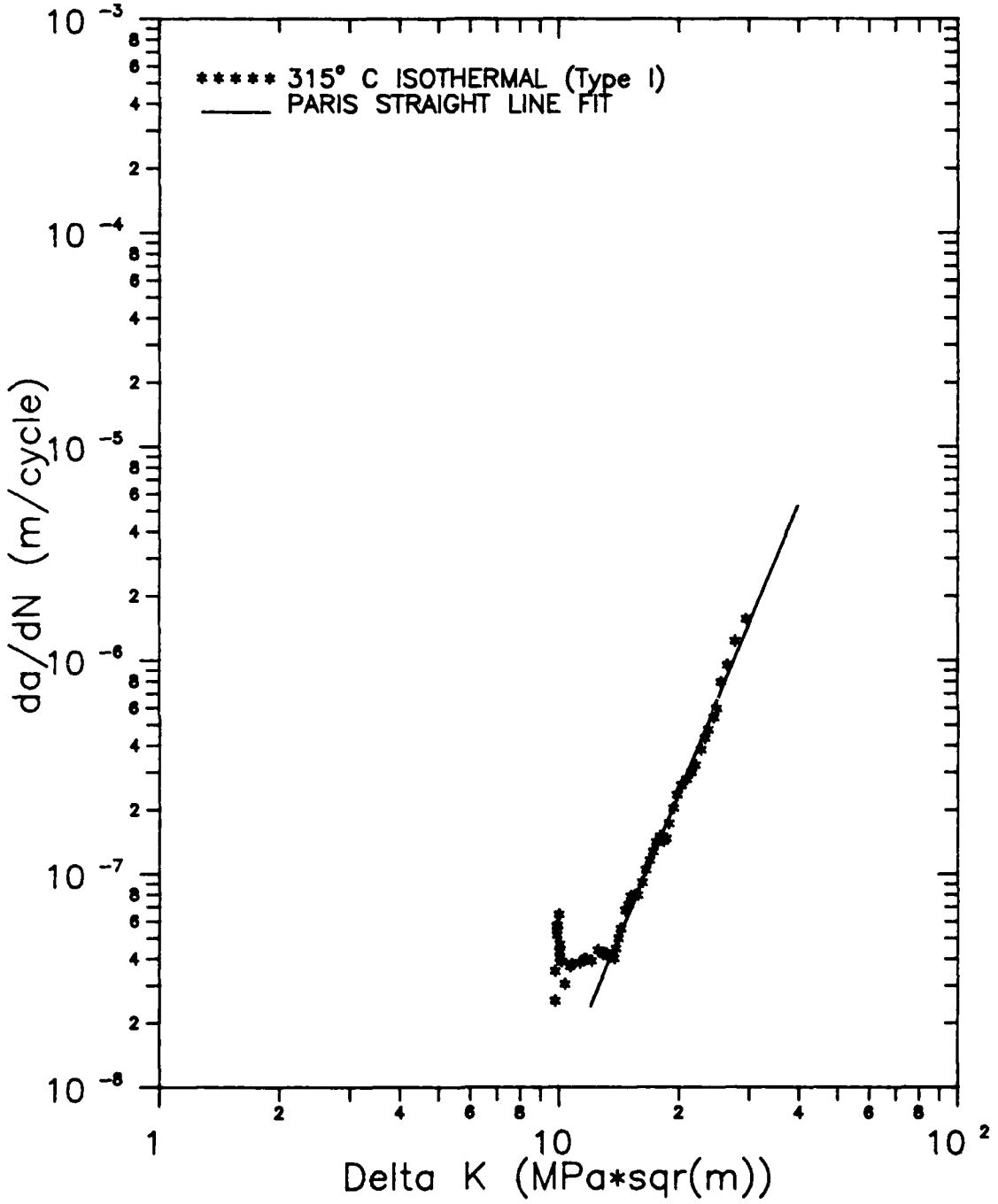

Fig. 28. 315° C crack growth data with straight line fit

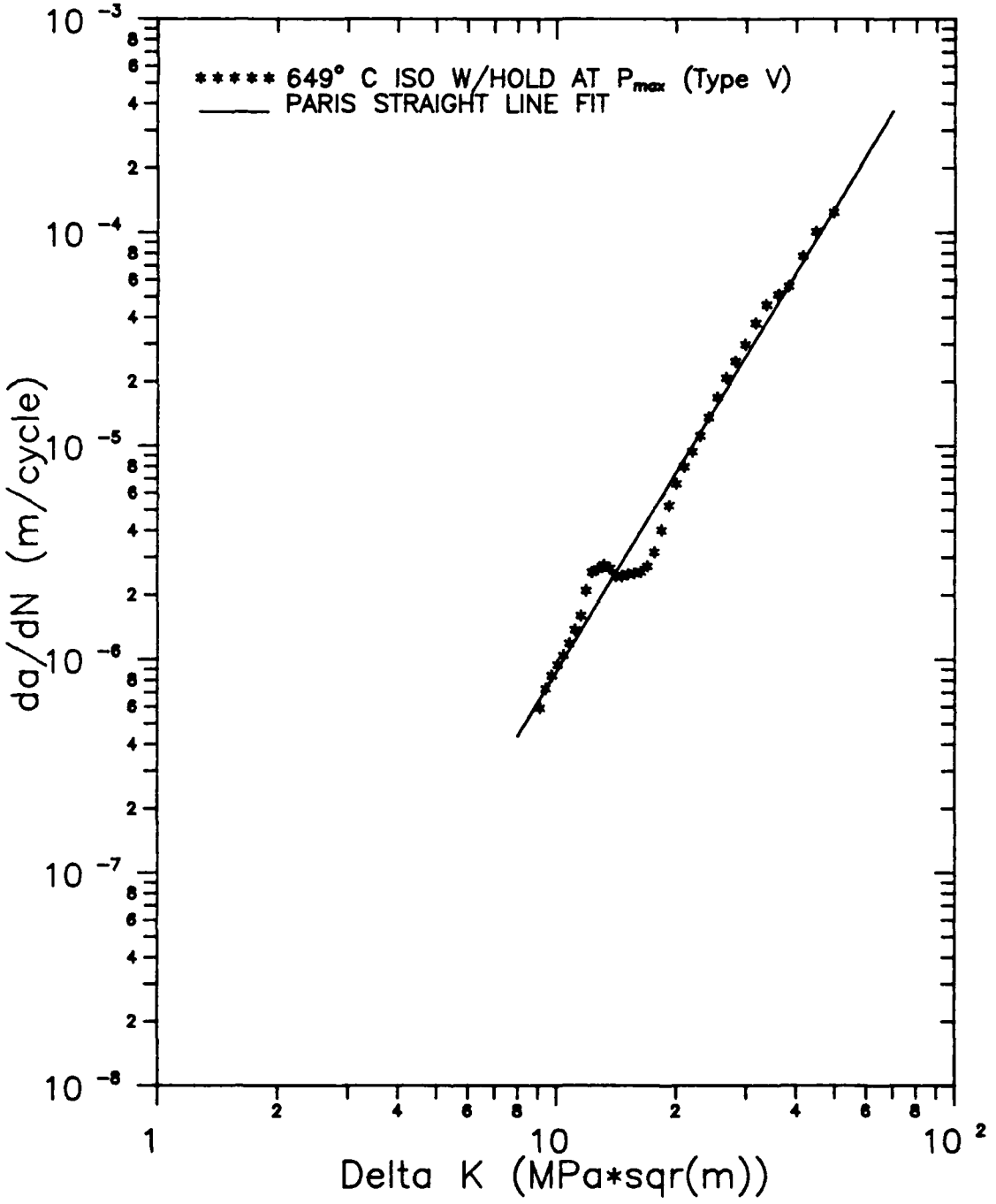

Fig. 29. 649° C isothermal w/hold at P_{max} crack growth data with straight line fit

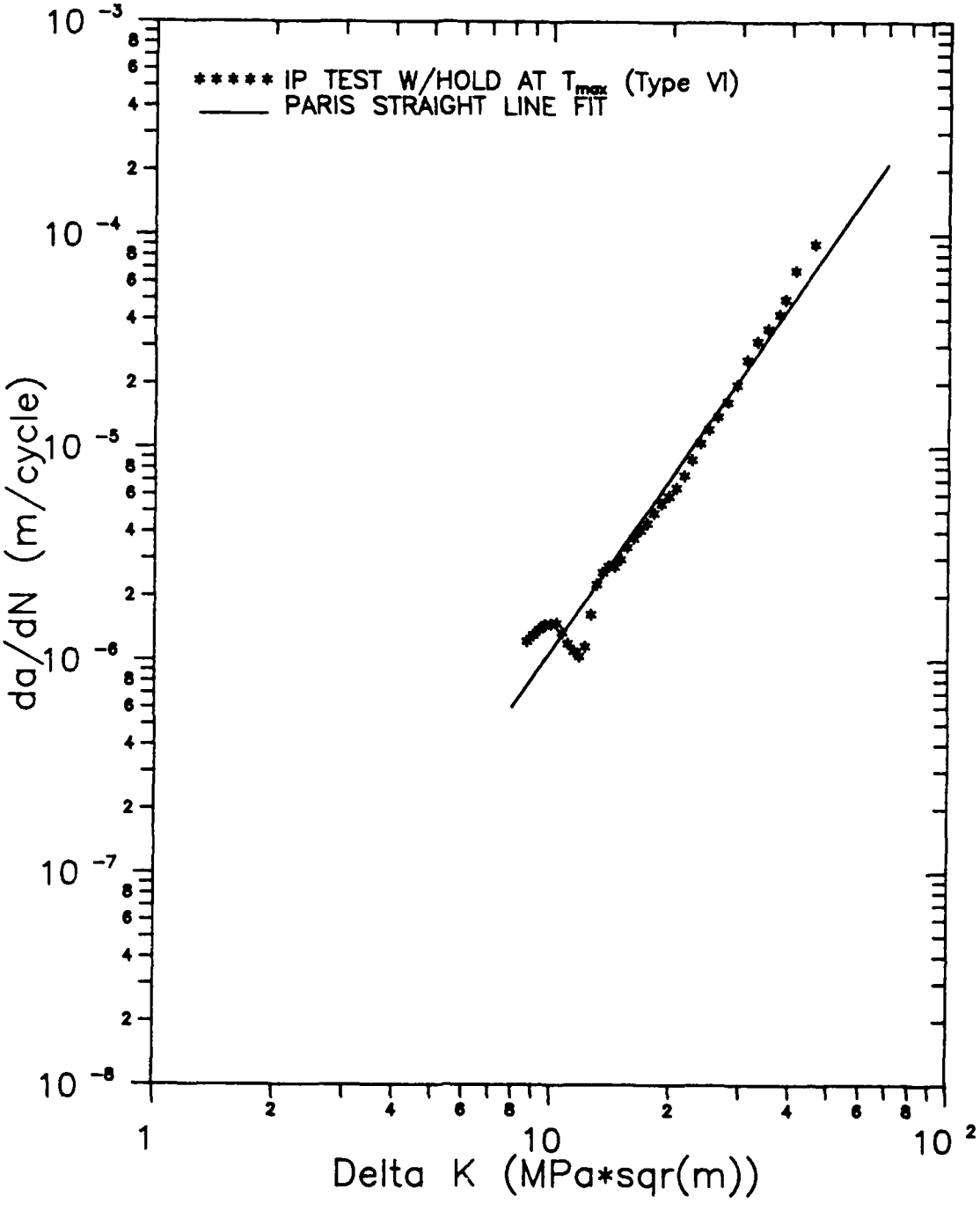

Fig. 30. In phase test w/hold at T_{max} crack growth data with straight line fit

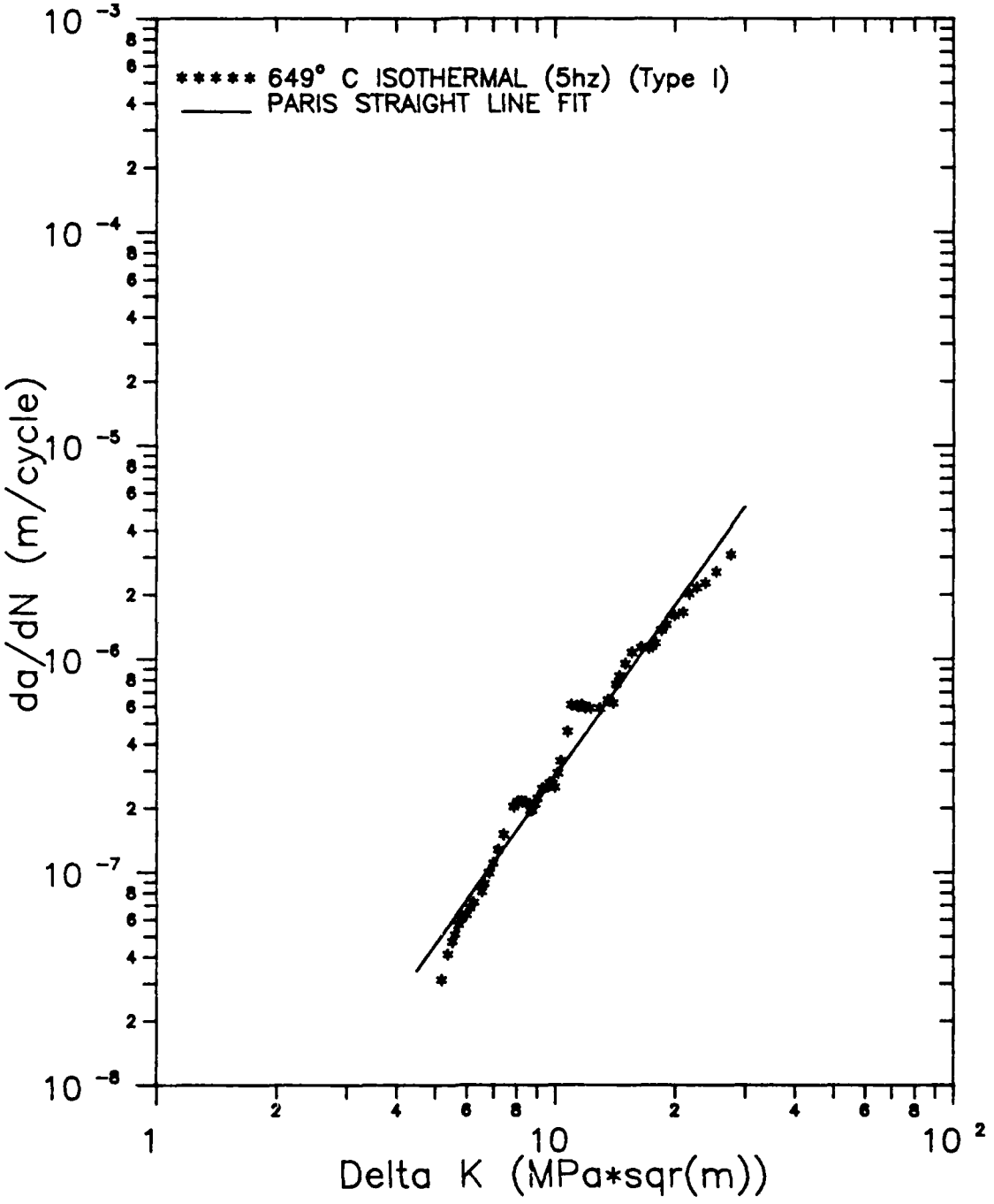

Fig. 31. 649° C isothermal 5 hz crack growth data and straight line fit

Environmental Effects on Crack Growth

A 180° phase (out of phase, type III) TMF test was conducted, and the results were compared with the 315° C isothermal fatigue test (type I) conducted by the Air Force Materials Laboratory. The out of phase (OP) test produced faster growth rate over the entire range of da/dN vs. ΔK data, as shown in Figure 32. The difference was greatest at the lower growth rates, e.g. for a ΔK of 11 MPa*sqr(m) the OP crack growth rate was approximately $5.0*10^{-7}$ m/cycle while the 315° C isothermal growth rate was approximately $4.0*10^{-8}$ m/cycle. The da/dN data of the two tests were separated by a factor of 12.5 at this point. On the other hand, the two da/dN vs. ΔK curves at the higher crack growth rates tended to merge together as da/dN and ΔK increased. For a ΔK of 25 MPa*sqr(m), the OP growth rate was approximately $3.0*10^{-6}$ m/cycle, while the 315° C isothermal growth rate was approximately $1.5*10^{-6}$ m/cycle. The da/dN data were separated by a factor of 2.0 at this point.

The maximum load for both of these tests occurred at 315° C, however the OP test produced faster crack growth rates. This phenomenon may be attributed to environmental degradation of the crack tip region during the periods of high temperature and minimum load in the OP test. This is most likely due to oxidation along the grain boundaries, which provided an easier path for the crack to propagate. Even though the crack did not grow at these low load/high

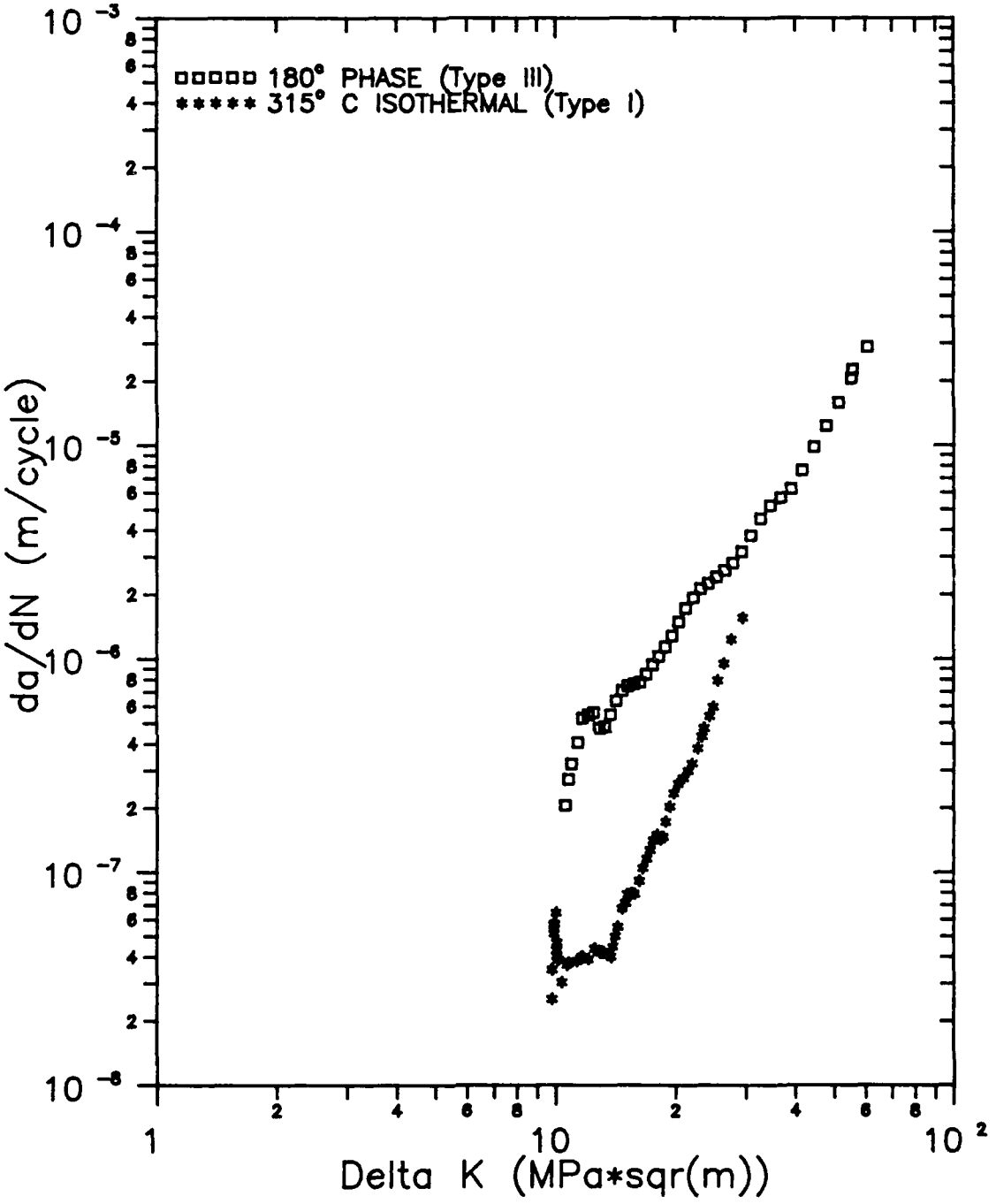

Fig. 32. Crack growth rates for 315° C isothermal and out of phase (180° phase)

temperature points in the cycle, the exposure to the 649° C temperature degraded (embrittled) the material around the crack tip. This might have caused the crack to grow faster during the next loading segment of the cycle than it did during the same loading segment of the 315° isothermal test.

It is also believed that the volume of material which is degraded is small, possibly on the order of the size of the plastic zone or smaller. If it is assumed that the size of this embrittled zone remains relatively constant during the course of the test, the merging of the two crack growth curves at higher da/dN values can be explained. At slow growth rates (10^{-8} to 10^{-7} m/cycle), the crack in the OP test was probably growing entirely within this embrittled zone during each cycle, as shown in Figure 33a. Due to the time-dependent nature of the environmental degradation, this zone will become even more brittle before the next loading cycle starts. This growth corresponds to a ΔK of 11 MPa*sqr(m) where there is the greatest difference between the growth rates of the two tests. On the other hand, during one cycle at higher growth rates (10^{-6} m/cycle), the crack in the OP test specimen probably was growing beyond the embrittled zone and into the surrounding non-embrittled material, as shown in Figure 33b. This growth corresponds to a ΔK equal to 25 MPa*sqr(m), where there is the least difference in the growth rates of the two tests. Therefore, in the OP test the effect of this embrittled zone became

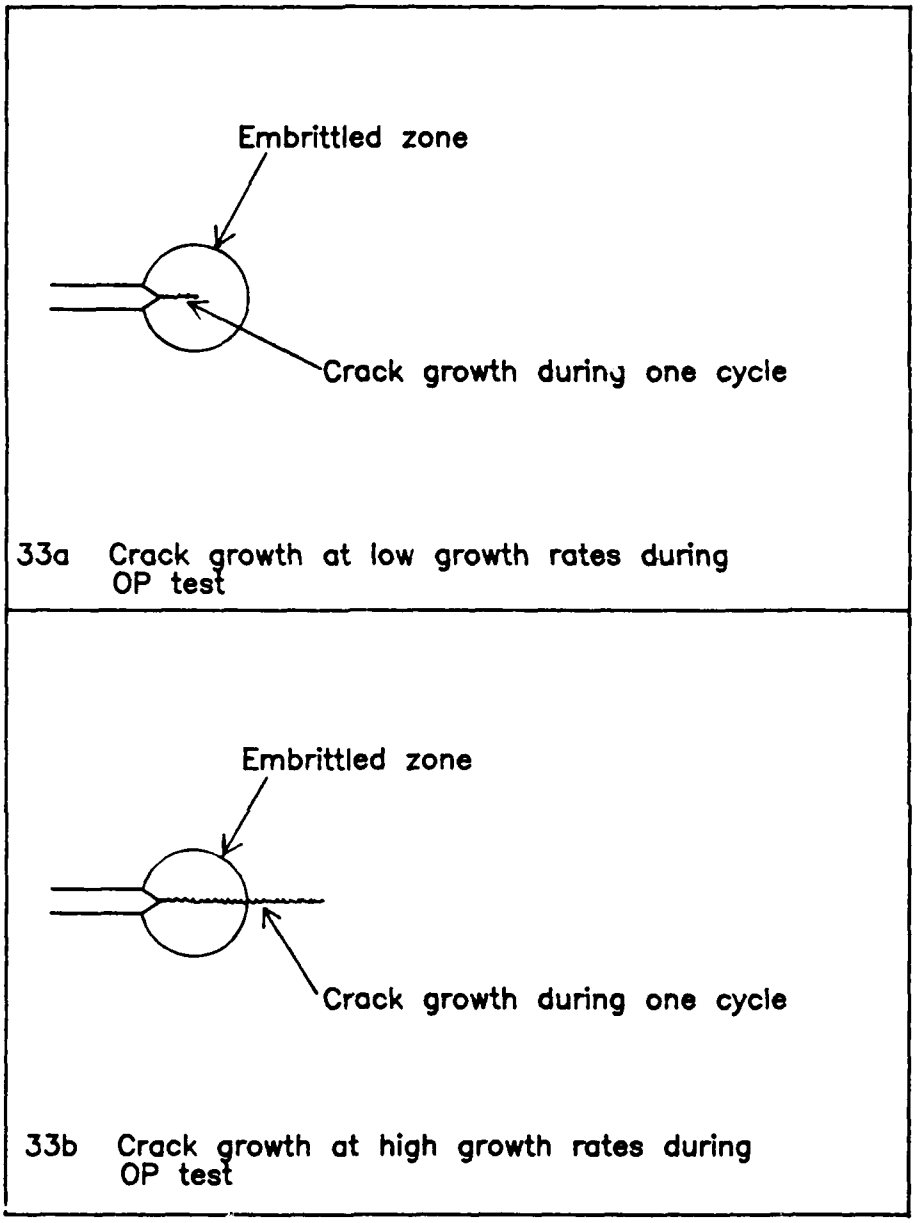

Fig. 33. Visualization of Embrittled Zone Caused by Environmental Degradation

less significant as the growth rate increased, and the OP crack growth data approached to that of the 315° C test, where embrittlement was not significant.

This environmental degradation is a time-dependent process. The amount of crack growth acceleration is dependent upon the amount of time which the crack tip is exposed to the damaging environment. At slow growth rates, the crack tip is repeatedly exposed to this environment and the growth rate is greatly accelerated as compared to the 315° C isothermal test. At higher growth rates, the crack tip is moving faster through the specimen and is therefore exposed to the environment for a shorter amount of time. This reduces the environmental degradation and brings the growth rate closer to that of the 315° C isothermal test. Further, the comparison between the OP test and the 315° C isothermal test suggests that this environmental degradation probably depends on the combination of temperature and load level. It is activated only under fluctuating load, since sustained load test at these temperatures (649° C) had no crack growth (29).

A further investigation of the environmentally enhanced crack growth is presented in Figure 34. This examines the frequency effect, or time-dependent effect, on the crack growth rate in this material during 649° isothermal fatigue tests (type I). Data from two tests, a 5 hertz and a .01 hertz, are compared here. Crack growth rates were much

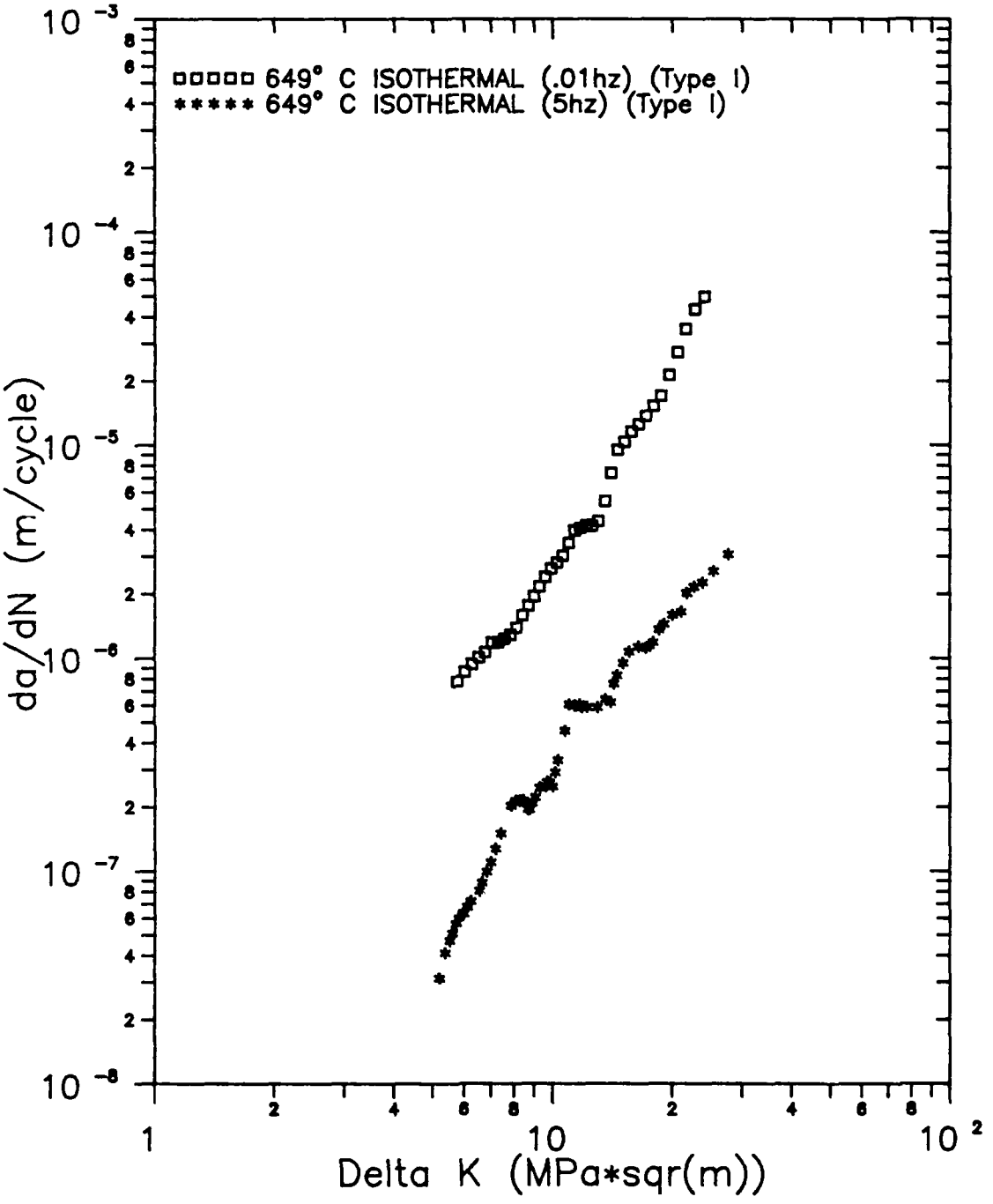

Fig. 34. Crack growth rates for 649° C isothermal tests, .01 hz and 5 hz

slower in the 5 hz test than in the .01 hz test. This may be attributed to the above mentioned environmental degradation (embrittlement) of the crack tip, during the high temperature/low load portion of the .01 hz test. This is the same phenomena as was seen in the OP test (type III). The crack grew more during the subsequent loading segment than it would have without the high temperature/low load embrittlement. The 5 hz test produced lower growth rates because of its much higher frequency as compared to the 0.01 hz test. The 5 hz test also contained the same low load/high temperature point in each cycle, but the test was conducted 500 times faster than the 0.01 hz test. Since embrittlement is a time-dependent behavior, each cycle of the 5 hz test was too fast to allow the embrittlement to occur, or fatigue growth was always ahead of embrittled zone as shown in Figure 33b.

The results of the 270° phase test (type IV) are compared with its counterpart from the OP test (type III); this comparison is shown in Figure 35. This figure shows that the crack growth rates for the 270° phase test were slightly higher than the crack growth rates of the OP test. This is probably due to the fact that the temperature varies, from 482° C to 649° C back to 482° C, during the loading segment of the 270° phase test. The temperature in the OP test drops, from 649° C to 315° C, during its loading segment. If it is assumed that crack growth occurs during

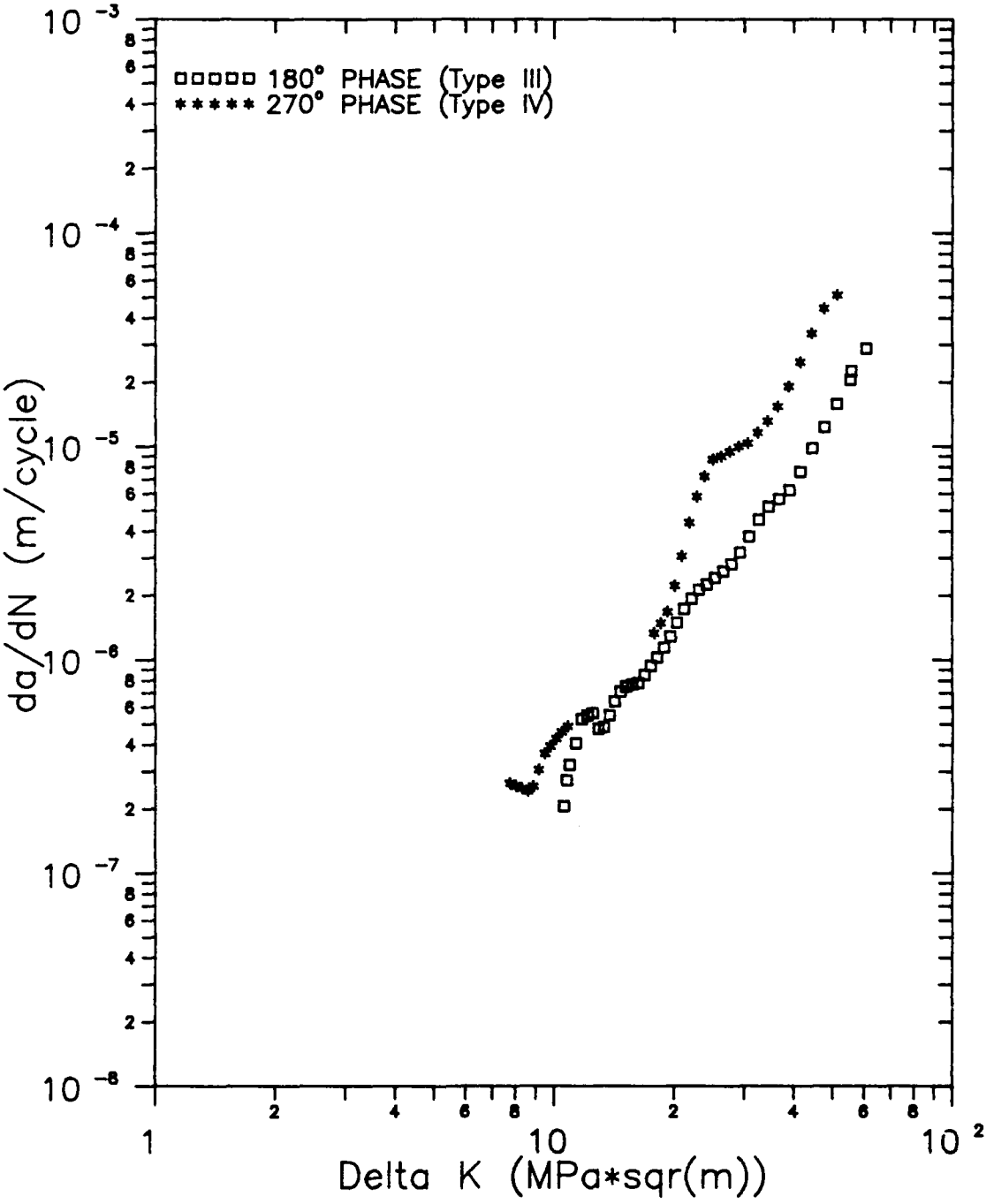

Fig. 35. Crack growth rates for 270° phase and 180° phase (OP)

the loading segment only, one would expect the 270° phase test to have faster growth rates due to the higher temperatures present during its loading segment. Heil (2:92-93) observed a similar phenomena in IN-718. His work showed higher growth rates during a 270° phase test than during a 90° phase test. Figure 4 shows that the two tests cover the same load vs. temperature paths but in opposite directions. Heil's crack growth prediction model assumed that crack growth occurred only during the loading portion of the cycle. Therefore, he concluded that the increased growth rates during his 270° phase test could be attributed to the higher temperatures present during its loading segment. This same type of phenomena appears to be present in the Ti_3Al alloy. This means that to effectively predict crack growth rates, the value of load and temperature as well as how the load and temperature are changing must be considered.

Creep Effects on Crack Growth As stated earlier, sustained load tests of this same Ti_3Al alloy by Staubs (29) showed no crack growth, for K from 20 to 50 MPa*sqr(m) for temperatures less than 700° C. An attempt was made to examine this phenomenon by inserting a hold time at the maximum load point of a 649° C isothermal fatigue test. The test consisted of a 48 second loading segment, a 48 second hold segment at maximum load, and a 48 second unloading segment as shown in Figure 22. This provided an opportunity

to look at the interaction of sustained load and fatigue phenomena at 649° C. As can be seen from Figure 36, the hold time test (type V) had slower crack growth rates than the 649° C isothermal test without the hold time (type I). This can be attributed to blunting of the crack tip during the load hold segment of the test. During each of the 48 second hold segments, the crack tip became blunted due to an increased yield zone as observed in creep crack growth tests. This caused the crack to grow less on the next loading portion than it would have without the hold time. Therefore, combined creep-fatigue interaction probably reduced crack growth rates as compared to the pure fatigue test at 649°. This effect is shown schematically in Figure 37. This figure shows how the crack would grow due to the combination of fatigue cycles and hold times under these conditions. During the first fatigue cycle, the slope of the crack length vs. time plot is equal to m; the subsequent hold time at maximum load blunts the crack tip and arrests crack growth. The slope of the crack length vs. time curve for the next fatigue cycle is less than m due to the blunting. This behavior continues, and the overall crack growth is shown to be less than that of pure fatigue.

An attempt was made to further examine the crack tip yielding and subsequent blunting as discussed above by conducting another type of test. This test consisted of 48 second load/temperature rise segment, a 48 second maximum

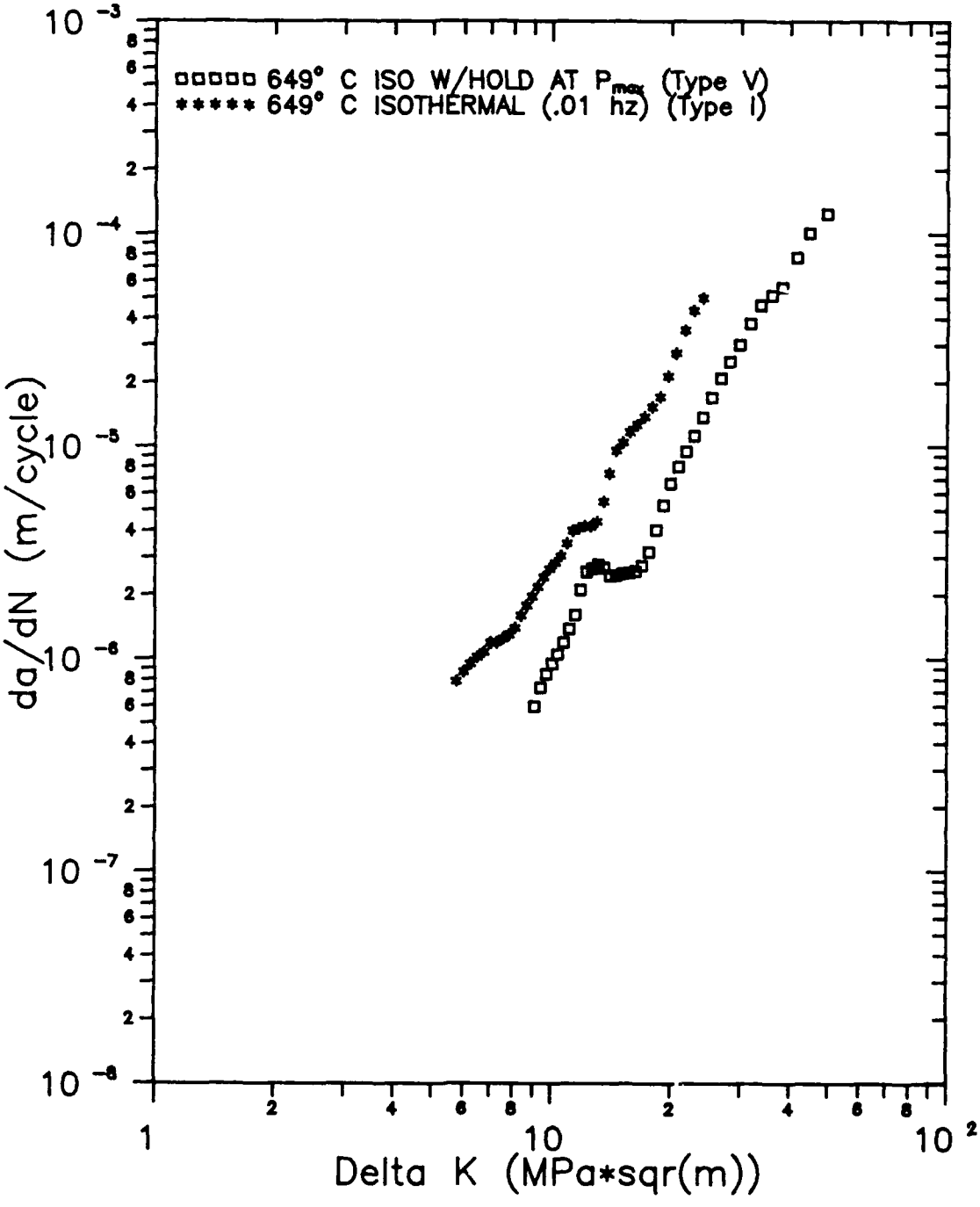

Fig. 36. Crack growth rates for 649° C isothermal (.01 hz) and 649° C isothermal with hold time at P_{max}

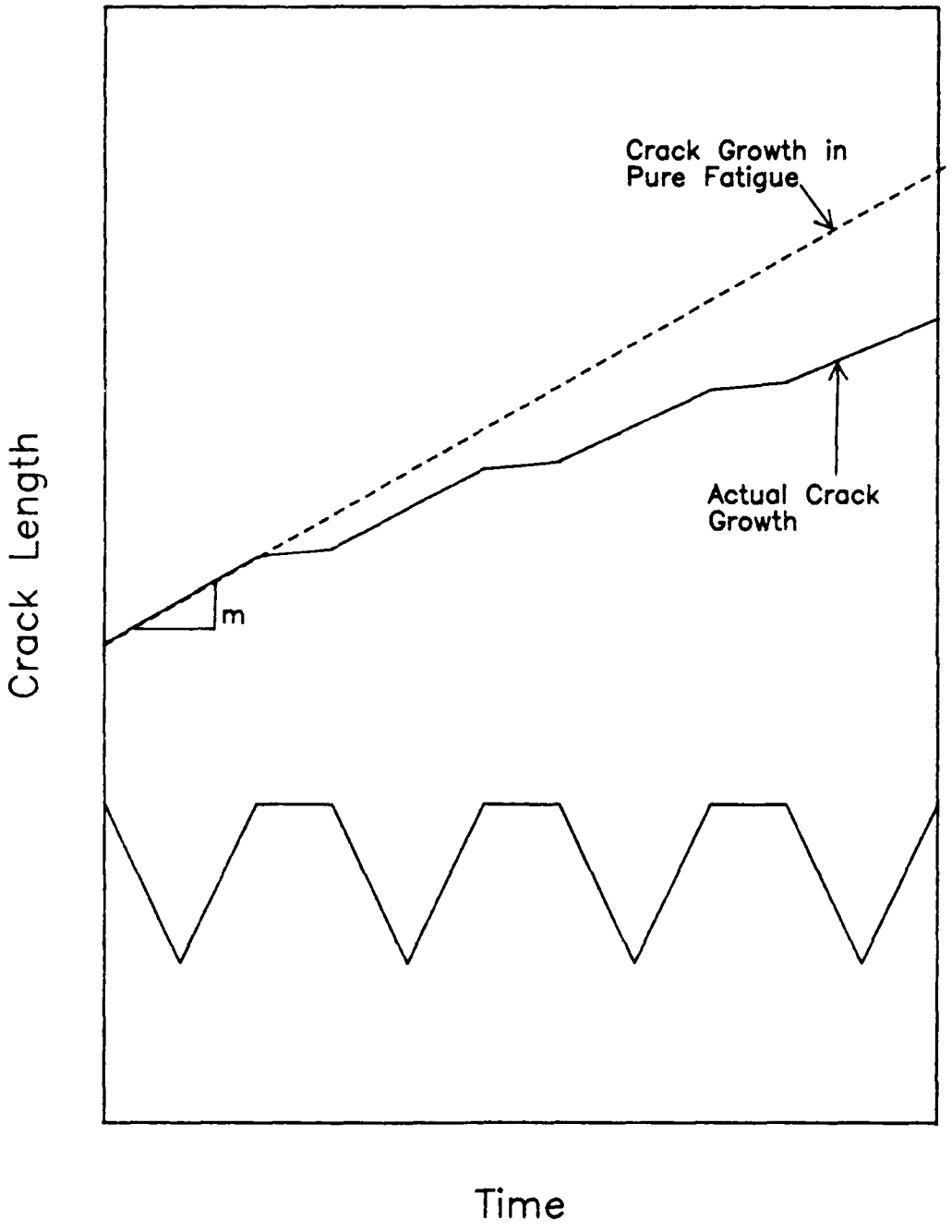

Fig. 37. Schematic of Crack Growth During Fatigue Test With Load Hold Time

temperature hold/unloading segment, and a 48 second minimum load hold/decreasing temperature segment as shown in Figure 23. The results from this test (type VI) are compared with the results from the 649° C test with load hold time (type V) and to the 0° phase test (type II) conducted by Pernot (5). These comparisons are presented in Figures 38 and 39 respectively.

The comparison of results of the type VI and type V will be discussed first. During the temperature hold (type VI) test, blunting due to yielding occurred while the temperature was held at 649° C and the load was reduced. Even though the load was decreasing while the temperature was held at 649° C, this test produced the da/dN vs. ΔK curve which was almost identical to 649° C load hold time test (type V). This indicates that the yielding of the crack tip probably occurred in a short time, when the temperature was held constant at 649° C and the load was still close to P_{max}. This is because yielding, and consequently blunting, occurs due to the combination of high temperature and high load. A shorter temperature hold time would probably produce the same blunting and reduced crack growth rates. This would be true as long as the load was reduced in a like manner as this test (ie 48 second unloading segment). In other words, a similar test with a 24 second hold time at 649° C and a 48 second unloading segment would probably produce similar results, but a test with a 24

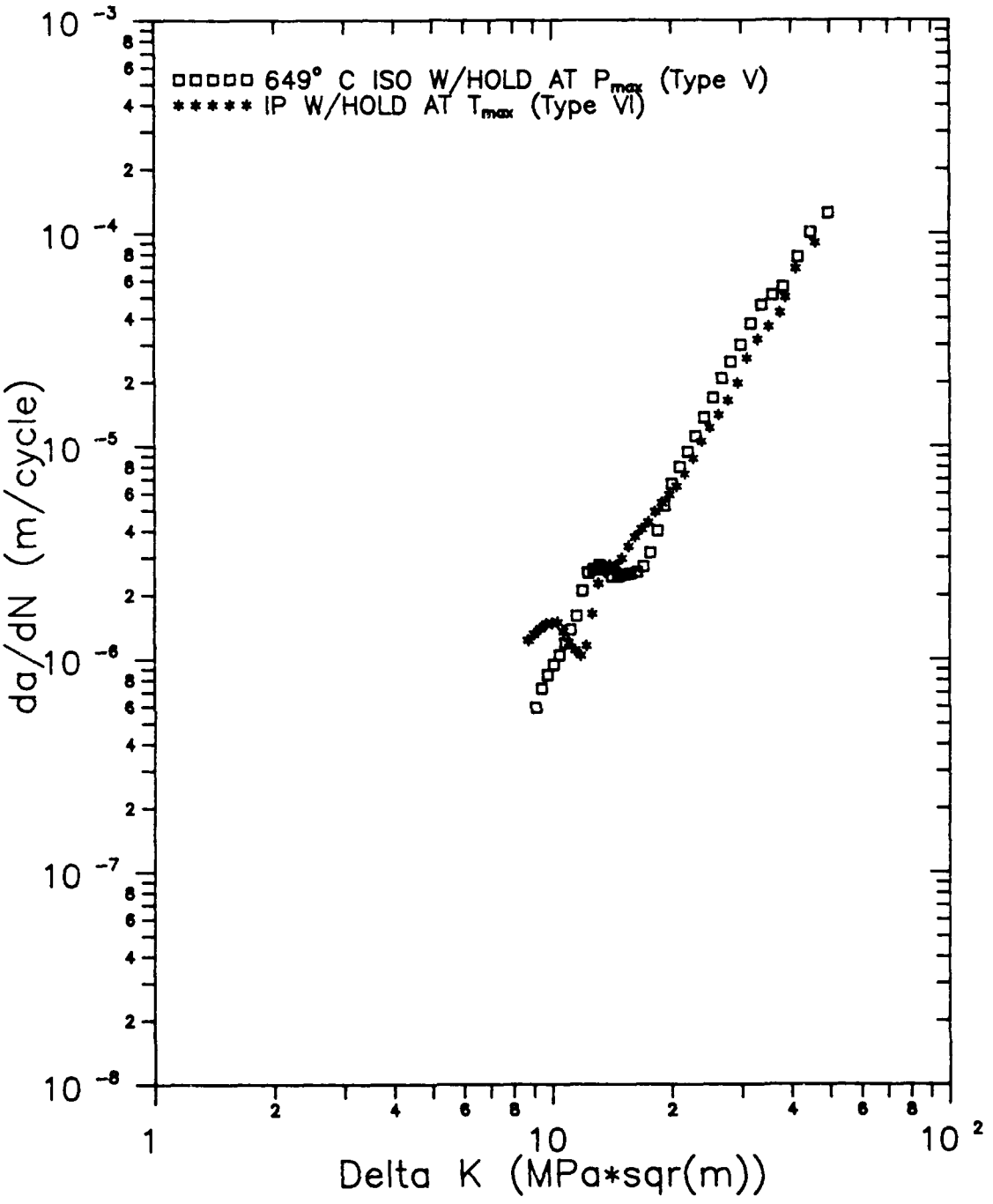

Fig. 38. Crack growth rates for 649° C isothermal w/hold at P_{max} and IP w/hold at T_{max}

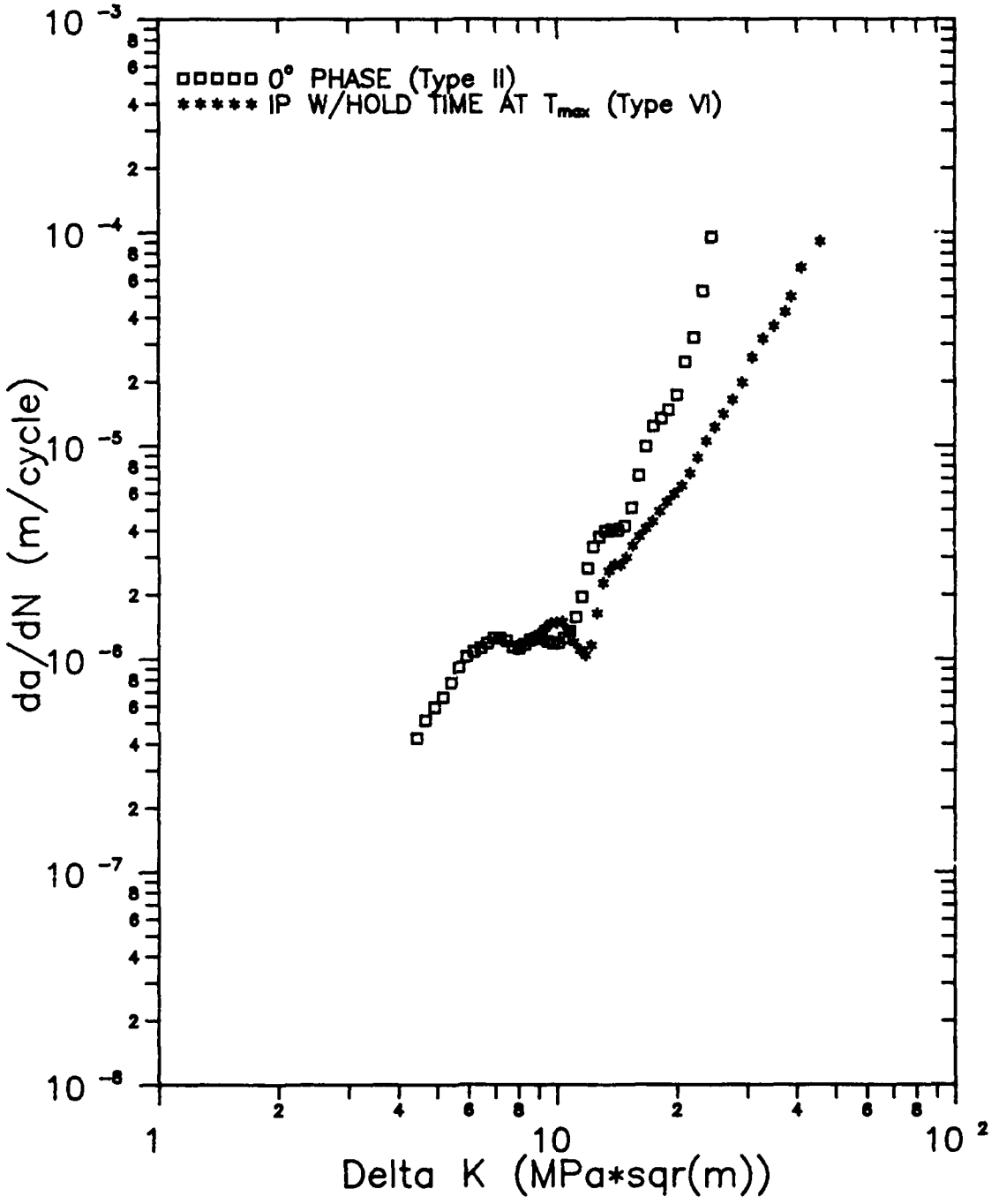

Fig. 39. Crack growth rates for in phase test and test with hold time at T_{max}

second hold at 649° C and a 12 second unloading segment may not. It is the interaction of the maximum temperature and maximum load which causes the blunting.

Comparison of the results of the type VI and type II tests will be presented next. This comparison is shown in Figure 39. For lower crack growth rates (less than 10^{-5} m/cycle), the temperature hold time test (type VI) produced the same da/dN vs. ΔK curve as the 0° phase test (type II). At higher crack growth rates, the two curves diverge with the type VI test having slower growth rates than the type II test. This divergence is probably due to the creep yielding during the temperature hold segment of the type VI test. This is the same retardation due to creep which was seen in the type V test. The type II test had no hold times at maximum load or maximum temperature, thus the yielding was not present, and the type II test had higher growth rates.

One explanation for the identical da/dN vs. ΔK curves at low growth rates is that environmental damage occurred toward the end of the temperature hold segment in the type VI test. At this point in the cycle, the crack tip was exposed to the same high temperature/low load conditions which caused the environmental degradation, and accelerated growth rates, seen in the type III test. The effect of the environmental degradation was great enough at low crack growth rates to cancel the creep blunting effects. At higher growth, rates the effect of the environmental

degradation diminished, and the creep blunting dominated. This same diminishing of the environmental effects was seen in the type III test. Both time-dependent phenomenon identified in the preceding comparisons appear to be present and in competition during the type IV test.

The above results have shown that two time-dependent phenomenon, environmental degradation and creep blunting, are present in this Ti_3Al alloy in the temperature range used in this investigation. In the case of IN-718 only the environmental degradation was present and Heil (2) was able to develop a simple linear summation model to predict crack growth. Due to the complex interaction of the two time dependent mechanisms in Ti_3Al alloy, Heil's model is not applicable to this material. More isothermal fatigue, isothermal fatigue with hold time, and TMF tests must be conducted. Crack growth data from these additional tests can be analyzed to determine the load and temperature conditions at which the two time-dependent phenomenon are present. The load and temperature conditions at which each of these phenomena dominate can also be determined. The interaction of the environment and creep effects must be understood before any attempt can be made to develop a crack growth prediction model for the Ti_3Al alloy.

Summary

For completeness, a comparison of crack growth rates from all the .01 hz tests is presented in Figure 40. A summary of the crack growth analysis accomplished during this present effort is given below. Crack growth rates in the Ti_3Al alloy have been found to be dependent on the following three factors:

1. Test temperature for isothermal fatigue tests or the temperature during the loading segment of the cycle for TMF tests. Crack growth rates increase with an increase in temperature.

2. Time-dependent environmental degradation (embrittlement) due to oxidation along the grain boundaries. This embrittlement accelerated the crack growth rates.

3. Crack tip yielding and subsequent blunting due to creep effects during the combination of high temperature/high load hold times. This blunting retarded the crack growth rates.

Some tests showed a clear dependence of crack growth rates on one of these three factors. Increasing the test frequency during 649° C isothermal fatigue tests (type I), from .01 hz to 5 hz, reduced crack growth rates because the

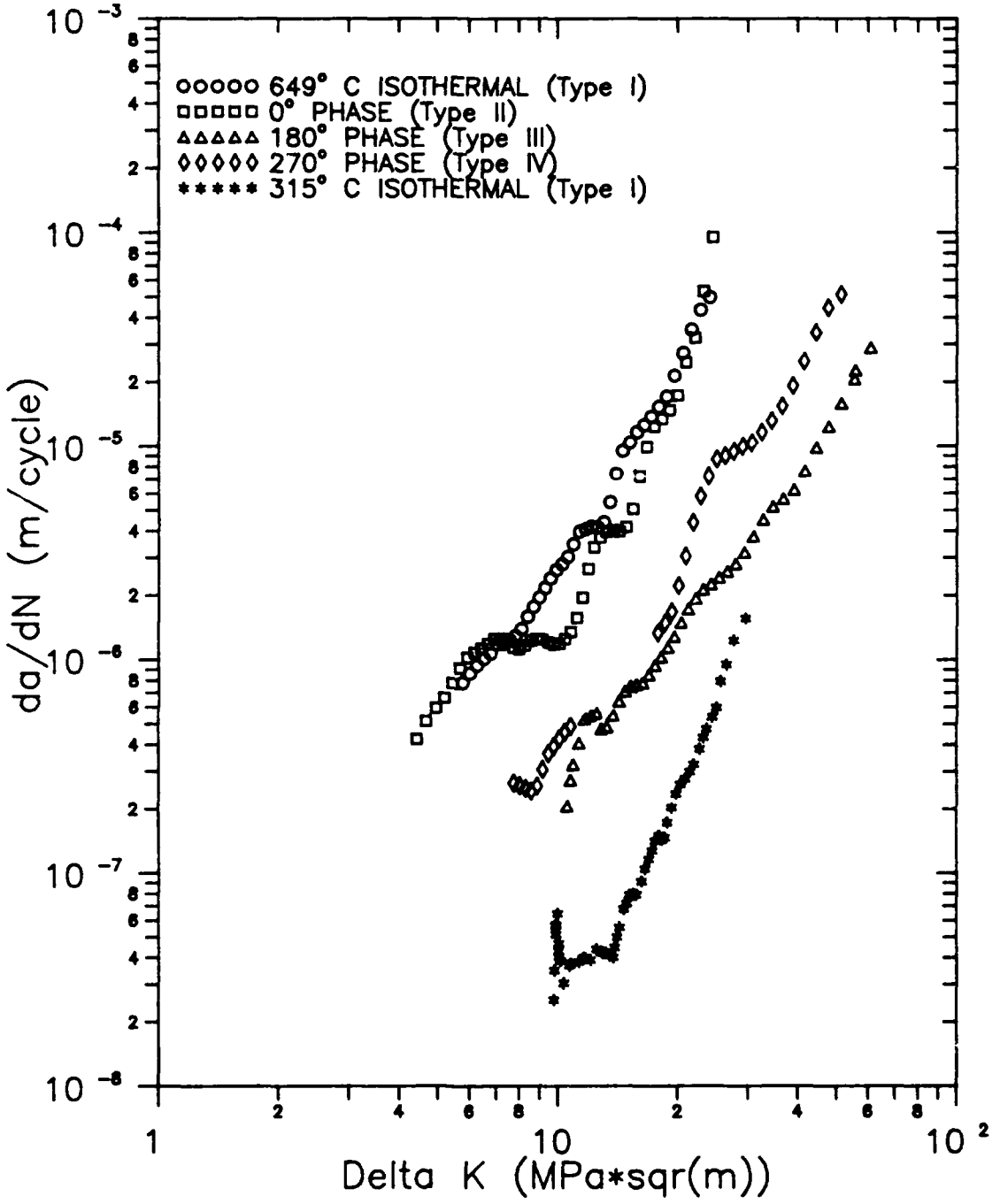

Fig. 40. Summary of the .01 hz crack growth data

time-dependent environmental degradation present in the .01 hz test was eliminated in the 5 hz test. By adding a hold time to a 649° C isothermal fatigue test (type V), crack growth rates were reduced due to blunting of the crack tip during the hold time. Another test, the IP test with hold time at T_{max} (type VI), showed that retardation due to blunting and acceleration due to environmental degradation can be present in the same test, each occurring at different points in the cycle. It is this complex interaction of the two competing damage mechanisms that made it difficult to develop a crack growth prediction model from the data available at present. Further, this interaction suggests that linear summation modeling, as employed in IN-718, may not be applicable in Ti_3Al.

Additional hold time tests must be conducted to determine the range of conditions where crack tip blunting is present. These tests should include shorter hold time tests at 649° C, and also hold time tests at other temperatures. Fatigue tests, at different temperatures and different frequencies, and in inert environments should be conducted to determine the range of conditions where environmental degradation is present. These tests could be followed by TMF tests. The data from all types of tests will be required before any model can be developed which can predict crack growth in this material during general TMF conditions, such as those seen in jet engine components.

The role of three commonly observed factors effecting crack growth behavior must be quantified. One possible scenario is shown in Figure 41. The three factors are cycle-dependent (pure fatigue phenomenon), time-dependent environmental effect, and time-dependent creep effect. Figure 41 shows crack growth rates, in general, for a constant temperature and constant ΔK. If a material behaves in a purely cycle-dependent mode, the crack growth rate is not a function of the cycle time. The crack growth rate in this case would remain constant as shown by the horizontal dashed line. Pure cycle-dependent behavior, over a broad range of cycle times, is rarely seen in engineering materials at elevated temperatures. Usually, one of two time-dependent factors effect crack growth rates. The first, environmental degradation, tends to increase crack growth rates. This phenomenon is shown by the upper curve. The cycle time at which this environmental effect begins to take place may vary with material, temperature, ΔK, and other factors. The second time-dependent factor, blunting due to creep, tends to decrease crack growth rates. This behavior is represented by the lower curve. Again, the cycle time at which a material deviates from cycle-dependent to time-dependent retardation due to blunting may vary with material, temperature, ΔK, and other factors.

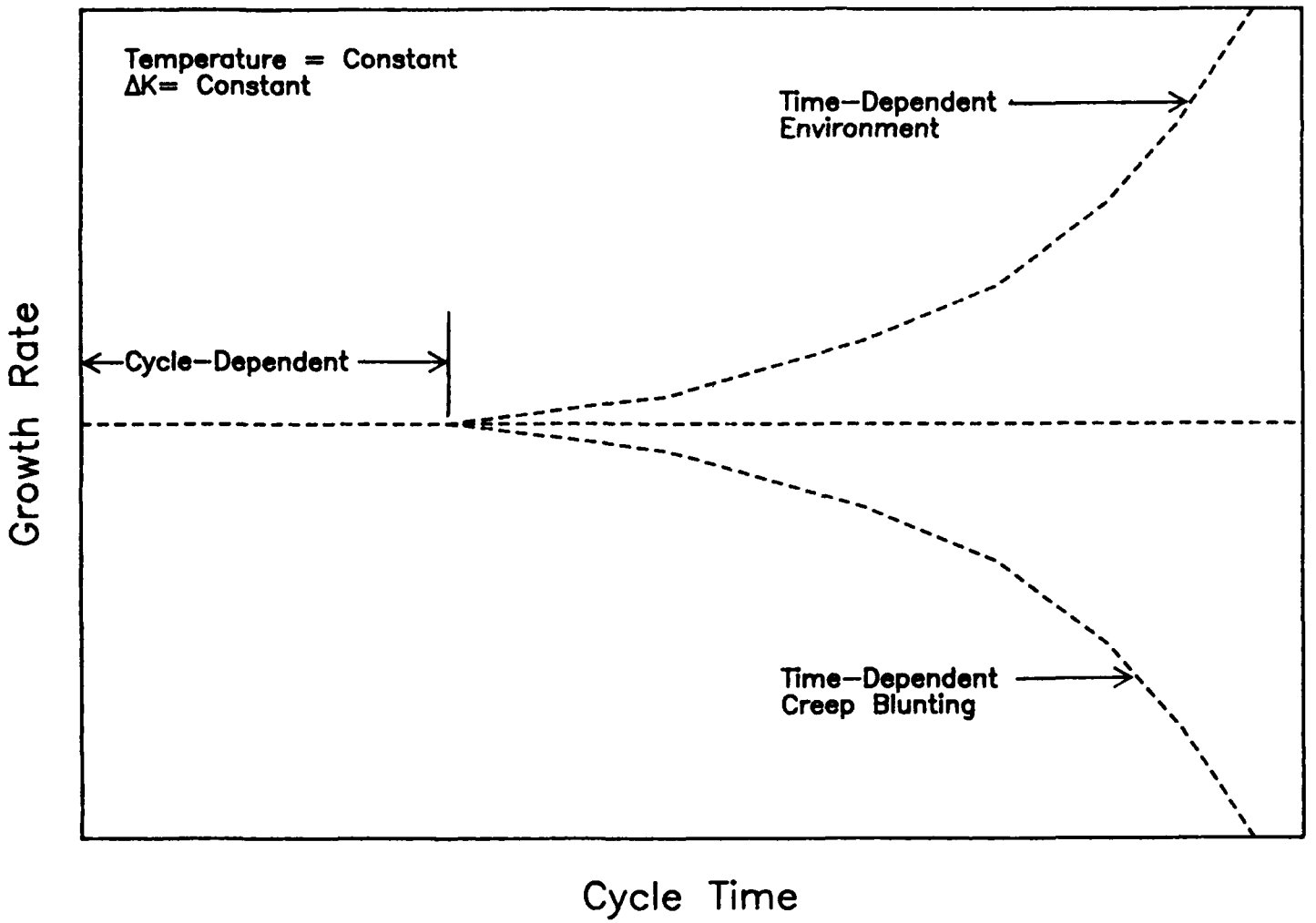

Fig. 41 Typical Crack Growth Rate vs. Cycle Time Curves

Figure 42 shows the interaction of these three factors present in the Ti_3Al alloy in a schematic way. This figure was constructed using data from the 649° C isothermal fatigue tests, and shows da/dN vs. cycle time at ΔK values of 10 MPa*sqr(m). Three such tests have been conducted, each with a different cycle time, and the da/dN corresponding to a ΔK of 10 Mpa*sqr(m) for each has been plotted in Figure 42. Solid lines have been used to connect the three data points. Dashed lines have been used to indicate where the data from additional tests with different cycle times would fall. As shown, if the cycle time is decreased (frequency increased), the crack growth rate will become entirely cycle-dependent and will level off to a constant value of da/dN. This is indicated by the dashed line from A to B. In pure fatigue tests, as cycle time is increased, cycle dependency gives way to environmental degradation and crack growth rates increase. This correspond to the curve from B to C. If the cycle time is increased enough, the fatigue test will then function as a sustained load test, and the crack growth rates will eventually fall off to zero due to crack tip blunting. This effect is shown from C to D. Similarly, if the cycle time is increased by adding long enough hold times to the fatigue cycle, the sustained load will dominate and crack tip blunting will cause the crack growth rates to fall off to zero. This effect of hold time is shown for two cases. The

curves, from E_1 to F_1, for a case where no data were available, and from E_2 to F_2, for the case where data were available, show this behavior.

The break points and the relations between these points, for the cycle-dependent, environmental degradation, and creep/blunting zones could not be determined explicitly in this present study. They are estimated, in Figure 42, as best as possible from the limited data available. More tests are required at 649° C to provide a clearer picture of where these break points are. Notice, that for a broad range of cycle times, it is expected that both environmental degradation and creep blunting of the crack tip will be present simultaneously. This is the type of interaction which must be explained before any modeling can be attempted. Once the 649° C behavior is understood, isothermal fatigue tests with and without hold times can be conducted at different temperatures and graphs similar to Figure 42 could be developed for other temperatures.

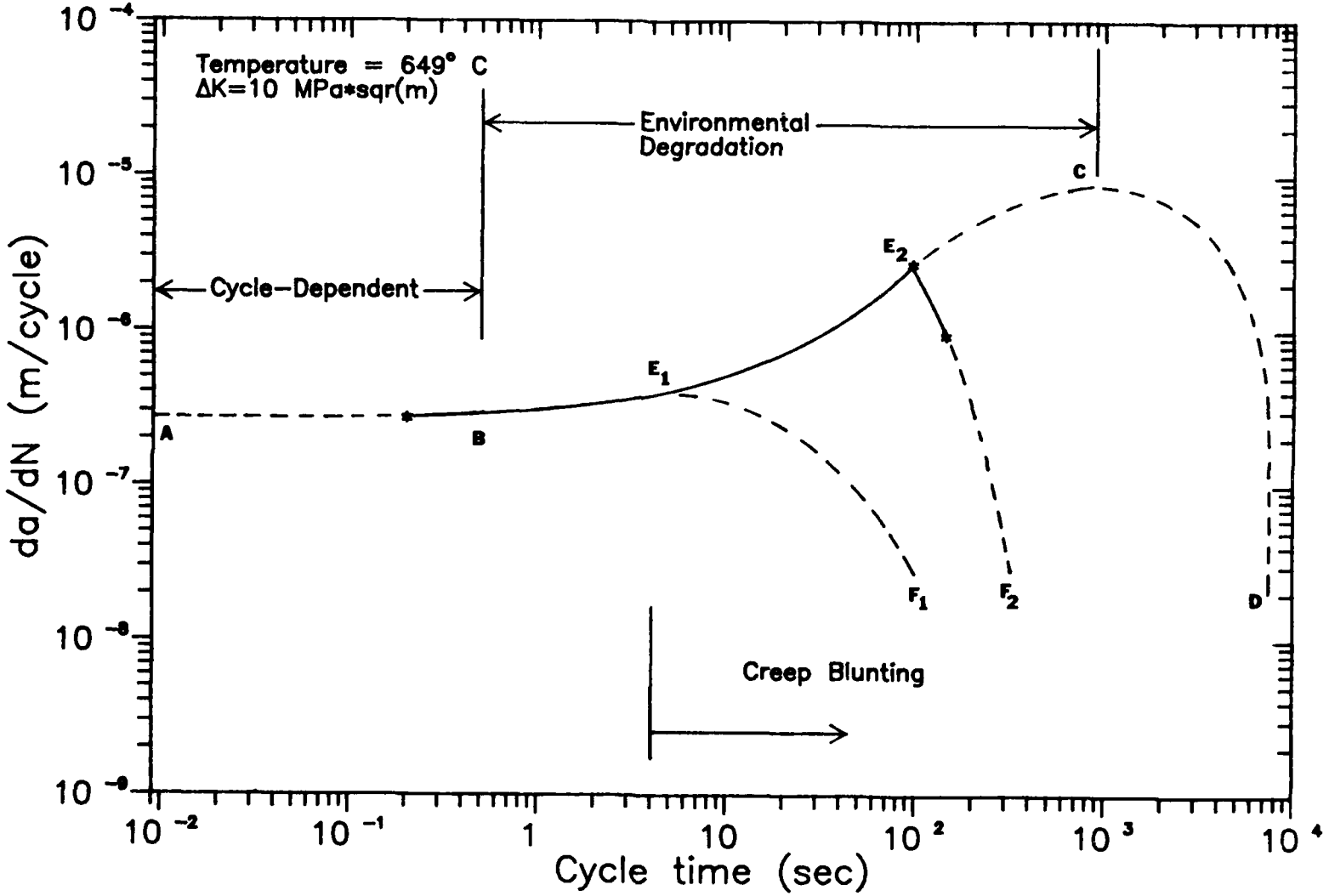

Fig. 42 Crack Growth Rate vs. Cycle Time for 649° C Isothermal Tests

VI. Conclusions and Recommendations

Three thermal-mechanical fatigue (TMF) tests and one isothermal fatigue test with hold time were conducted using compact tension specimen machined from the titanium-aluminide alloy, Ti_3Al. Crack growth data was gathered during these tests using a D.C. voltage drop technique. Crack growth data from these tests were compared with data from previous isothermal fatigue and TMF tests of the same material. The da/dN vs. K data from all these tests correlated very well with the Paris equation.

Three factors effecting crack growth rates were found to be present in this material in the temperature range investigated (315-649° C). Pure cycle-dependent crack growth was seen during 315° C isothermal fatigue and 649° C isothermal fatigue (5 hz) tests. Crack growth rates increased with an increase in temperature in the cycle-dependent region. Two types of time-dependent behavior was present. Environmentally enhanced crack growth was seen in a 649° C isothermal fatigue test (.01 hz) and also in a 180° phase TMF test. In both cases, the crack growth rate was accelerated due to oxidation along grain boundaries. Blunting of the crack tip, due to creep effects, was seen when a 48 second hold time at maximum load was added to the .01 hz isothermal fatigue test. This blunting caused retarded crack growth rates in the hold time test. During a 0° phase

test with a 48 second hold time at maximum temperature, both of these time-dependent factors were present and were competing with each other. The presence of the two kinds of time-dependent mechanisms made it impossible to develop a crack growth prediction model for this material with the data available at present.

It is recommended that additional tests be conducted before any modeling is attempted. The following tests will be required to determine the range of conditions at which these two time-dependent damage mechanisms are present. Additional load hold time tests should be conducted at 649° C, these tests should include hold times shorter than the 48 seconds used here. Load hold time tests at temperatures lower than 649° C should also be conducted. These tests will help define the conditions where the creep blunting is present. Additional fatigue tests at different temperatures and environments should be conducted to further understand the environmental degradation phenomena. After these time-dependent phenomena are better understood, more TMF tests can be conducted to complete the data necessary for modeling.

Bibliography

1. Jordan, E.H. and Meyers, G.J., "Fracture Mechanics Applied to Nonisothermal Fatigue Crack Growth, Eng. Frac. Mech., Vol 23, No.2, 1986.

2. Heil, Michael L., Crack Growth in Alloy 718 Under Thermal-Mechanical Cycling, PhD dissertation, AFIT/DS/AA/86-1, School of Engineering, Air Force Institute of Technology (AU), Wright-Patterson AFB OH, December 1986.

3. Aeronautical Systems Division, Air Force Systems Command, Fatigue and Fracture of Titanium-Aluminides, Wright-Patterson AFB OH, February 1985.

4. Venkataraman, S., Elevated Temperature Crack Growth Studies of Advanced Titanium-Aluminides, Technical Report No. AFWAL-TR-87-4103, Wright-Patterson AFB OH, September 1987.

5. Pernot, John J., Thermal Mechanical Testing of a Titanium-Aluminide Alloy, MS thesis, AFIT/GAE/AA/78D-18, School of Engineering, Air Force Institute of Technology (AU), Wright-Patterson AFB OH, December 1987.

6. Broek, David, Elementary Engineering Fracture Mechanics, Netherlands, Martin Nijhoff Publishers, 1986.

7. Reidel, Herman, Fracture at High Temperatures, Springer-Verlay, New York, 1986.

8. Tiev, J.K., Nair, S.V. and Nardone, V.C., "Creep-Fatigue Interaction in Structural Alloys", Flow and Fracture at Elevated Temperatures, American Society for Metals, 1985.

9. Coffin, L.F. Jr., "The Effect of High-Vacuum on the Low Cycle Fatigue Law", Met. Trans., 1972.

10. James, L.A., "Some Questions Regarding the Interactions of Creep and Fatigue", Journal of Eng. Mat. and Tech., July 1976

11. Raj, R., "Mechanisms of Creep-Fatigue Interaction", Flow and Fracture at Elevated Temperatures, American Society for Metals, 1985.

12. Reidel, Herman, "Creep Crack Growth", Flow and Fracture Elevated Temperatures, American Society for Metals, 1985.

13. Larsen, J.M. and Nicholas T., "Cumulative-Damage Modeling of fatigue Crack Growth in Turbine Engine Materials", Eng. Frac. Mech, 22, 1985.

14. Nicholas, T., Weerasooriya, T. and Ashbaugh, N.E., "A Model for Creep/Fatigue Interaction in Alloy 718", ASTM STP 905, Fracture Mechanics, Sixteenth Vol, ASTM, 1986.

15. Nicholas, T. and Weerasooyiya, T. "Hold-Time Effects in Elevated Temperature Fatigue Crack Propagation", ASTM STP 905, Fracture Mechanics, Sixteenth Vol., ASTM, 1986.

16. Floreen, S., "The Creep Fracture of Wrought Nickel-Base Alloys by a Fracture Mechanics Approach", Met. Trans., Vol 6A, 1975.

17. Coles, A., Johnson, R.E. and Popp, H.G., "Utility of Surface-Flawed Tensile Bars in Cycle Life Studies", J. of Eng. Mat. Tech., Vol 98, 1976.

18. Harmon, D.A. and Burns, J.G., "Development of an Elevated Temperature Crack Growth Routine", AIAA, 1988.

19. Paris, P.C. and Erdogan, F., "A Critical Analysis of Propagation Laws", J. of Basic Eng. Trans. ASME, Series D., 55, 1963.

20. Sims, D.L. and Haake, F.K., Evaluation of Crack Growth in Advanced P/M Alloys, AFWAL-TR-79-4160, Wright-Patterson AFB OH, 1980.

21 Utah, D.A., Crack Modeling in an Advanced Powder Metallurgy Alloy, AFWAL-TR-80-4098, 1981.

22. Wei, R.P. and Landes, J.D., "Correlation Between Sustained-Load and Fatigue Crack Growth in High-Strength Steels", Mat. Res. and Stand., Vol 19 1969.

23. Solomon, H.D., "Corrosion Fatigue, NACE-2, NACE, 1972.

24. Hartios,G.K., Miller, D.L. and Nicholas, T., "Sustained Load Crack Growth in INconel 718 Under Nonisothermal Conditions", Trans. of the ASME, Vol 107, 1985.

25. ASTM, 1985 Annual Book of ASTM Standards, American Society for Testing and Materials, 1985.

26. Johnson, H.H., "Calibrating the Electric Potential Method for Studying Slow Crack Growth", Mat. Res. and Stand., Vol 5, No.9, 1965.

27. Hartman, G.A. and Johnson, D.A., "D-C Electric Potential Method Applied to Thermal/Mechanical Fatigue Crack Growth", Experimental Mechanics, March 1987.

28. Larsen, J.M., "An Automated Photomicroscopic System for Monitoring Growth of Small Fatigue Cracks", Fracture Mechanics, Vol 17, ASTM STP 905, ASTM, 1986.

29. Staubs, E., Investigation of Crack Growth in Titanium-Aluminide at Elevated Temperatures, MS thesis, AFIT/GAE/AA/88D-36, School of Engineering, Air Force Institute of Technology (AU), Wright-Patterson AFB OH, December 1988.

VITA

Captain David G. Burgess was born on [redacted] He graduated from Southland High School, [redacted] in 1973. He entered the United States Air Force in May 1978. He received a Bachelor of Science in Mechanical Engineering, from the University of Missouri-Rolla in 1984. He received a commission in the USAF in August 1984. He worked as a test engineer in the 3246 Test Wing, Eglin AFB Fla, from August 1984 until May 1987 when he entered the School of Engineering, Air Force Institute of Technology.

[redacted]

UNCLASSIFIED
SECURITY CLASSIFICATION OF THIS PAGE

REPORT DOCUMENTATION PAGE

Form Approved OMB No. 0704-0188

1a. REPORT SECURITY CLASSIFICATION: UNCLASSIFIED	1b. RESTRICTIVE MARKINGS
2a. SECURITY CLASSIFICATION AUTHORITY	3. DISTRIBUTION/AVAILABILITY OF REPORT: Approved for public release; distribution unlimited.
2b. DECLASSIFICATION/DOWNGRADING SCHEDULE	
4. PERFORMING ORGANIZATION REPORT NUMBER(S): AFIT/GAE/AA/88D-3	5. MONITORING ORGANIZATION REPORT NUMBER(S)
6a. NAME OF PERFORMING ORGANIZATION: School of Engineering; 6b. OFFICE SYMBOL (If applicable): AFIT/ENY	7a. NAME OF MONITORING ORGANIZATION
6c. ADDRESS (City, State, and ZIP Code): Air Force Institute of Technology (AU) Wright-Patterson, AFB, OH 45433-6583	7b. ADDRESS (City, State, and ZIP Code)
8a. NAME OF FUNDING/SPONSORING ORGANIZATION: Materials Lab, Ceramic and Metals Division; 8b. OFFICE SYMBOL (If applicable): AFWAL/MLLN	9. PROCUREMENT INSTRUMENT IDENTIFICATION NUMBER
8c. ADDRESS (City, State, and ZIP Code): AFWAL/MLLN Wright-Patterson, AFB, OH 45433-6583	10. SOURCE OF FUNDING NUMBERS: PROGRAM ELEMENT NO. / PROJECT NO. / TASK NO / WORK UNIT ACCESSION NO.

11. TITLE (Include Security Classification): See BOX 19

12. PERSONAL AUTHOR(S): David G. Burgess, Capt., USAF

13a. TYPE OF REPORT	13b. TIME COVERED	14. DATE OF REPORT (Year, Month, Day)	15. PAGE COUNT
MS Thesis	FROM _____ TO _____	1988 December	110

16. SUPPLEMENTARY NOTATION

17. COSATI CODES			18. SUBJECT TERMS (Continue on reverse if necessary and identify by block number)
FIELD	GROUP	SUB-GROUP	Thermal-Mechanical Fatigue, Environmental Degradation, Creep, Fracture, Titanium Alloys
20	11		

19. ABSTRACT (Continue on reverse if necessary and identify by block number)

Title: CRACK GROWTH OF A TITANIUM-ALUMINIDE ALLOY UNDER THERMAL-MECHANICAL FATIGUE

Thesis Chairman: Shankar Mall
Professor of Aeronautics and Astronautics

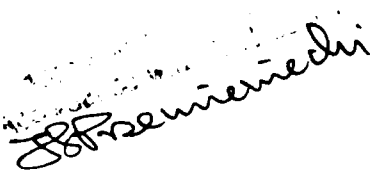

20. DISTRIBUTION/AVAILABILITY OF ABSTRACT: UNCLASSIFIED/UNLIMITED ☒ SAME AS RPT. ☐ DTIC USERS	21. ABSTRACT SECURITY CLASSIFICATION: UNCLASSIFIED
22a. NAME OF RESPONSIBLE INDIVIDUAL: Shankar Mall	22b. TELEPHONE (Include Area Code): (513)255-5533; 22c. OFFICE SYMBOL: AFIT/ENY

DD Form 1473, JUN 86 — Previous editions are obsolete. — SECURITY CLASSIFICATION OF THIS PAGE

UNCLASSIFIED

New materials must be developed in order to increase the operating temperature of Air Force gas turbines. One of the materials under consideration is a titanium-aluminide alloy, Ti_3Al. Before this material can be used, its behavior under combined thermal-mechanical fatigue (TMF) conditions must be understood.

To understand this behavior, three 315-649° C TMF tests and one 649° C isothermal fatigue test with load hold time were conducted. Crack growth data from these tests were compared with each other as well as with crack growth data from four previous TMF and isothermal fatigue tests of the same material.

Two competing time-dependent crack growth mechanisms were present. Environmental degradation of the crack tip occurred when the material was exposed to points of maximum temperature and minimum load in the cycle. This accelerated the crack growth rates. Blunting of the crack tip due to creep occurred during hold times of maximum temperature and maximum load. This retarded crack growth rates.

Further TMF and isothermal fatigue tests are required to fully understand under what conditions these two time-dependent phenomena are present. This understanding is required before any TMF crack growth prediction model can be developed for this material.